A hybrid method for computing the Schrödinger equations with periodic potential with band-crossings in the momentum space

Lihui Chai[*] Shi Jin[†] Peter A. Markowich[‡]

Abstract

We propose a hybrid method which combines the Bloch decomposition-based time splitting (BDTS) method and the Gaussian beam method to simulate the Schrödinger equation with periodic potentials in the case of band-crossings. With the help of the Bloch transformation, we develop a Bloch decomposition-based Gaussian beam (BDGB) approximation in the momentum space to solve the Schrödinger equation. Around the band-crossing a BDTS method is used to capture the inter-band transitions, and away from the crossing, a BDGB method is applied in order to improve the efficiency. Numerical results show that this method can capture the inter-band transitions accurately with a computational cost much lower than the direct solver. We also compare the Schrödinger equation with its Dirac approximation, and numerically show that, as the rescaled Planck number $\varepsilon \to 0$, the Schrödinger equation converges to the Dirac equations when the external potential is zero or small, but for general external potentials there is an $O(1)$ difference in between the solutions of the Schrödinger equation and its Dirac approximation.

[*]Department of Mathematics, University of California, Santa Barbara, USA (chai@ucsb.edu)

[†]Department of Mathematics, University of Wisconsin-Madison, Madison, WI 53706, USA (sjin@wisc.edu) and Institute of Natural Sciences, School of Mathematical Science, MOELSEC and SHL-MAC, Shanghai JiaoTong University, Shanghai 200240, China. This authors research was supported by NSF grants DMS-1522184 and DMS-1107291: RNMS KI-Net, by NSFC grant No. 91330203, and by the Office of the Vice Chancellor for Research and Graduate Education at the University of Wisconsin-Madison with funding from the Wisconsin Alumni Research Foundation.

[‡]Division of Math and Computer Sciences and Engineering, King Abdullah University of Science and Technology, Thuwal 23955-6900, Kingdom of Saudi Arabia (peter.markowich@kaust.edu.sa)

1 Introduction: The Schrödinger equation with periodic potential

The linear Schrödinger equation with periodic potentials is an important model in solid state physics. It describes the motion of electrons in a crystal with a lattice structure. We consider the following Schrödinger equation in the semiclassical scaling

$$\mathrm{i}\varepsilon\partial_t\psi^\varepsilon(t,\boldsymbol{r}) = -\frac{\varepsilon^2}{2}\Delta_{\boldsymbol{r}}\psi^\varepsilon(t,\boldsymbol{r}) + \left(V_\Gamma\left(\frac{\boldsymbol{r}}{\varepsilon}\right) + U(\boldsymbol{r})\right)\psi^\varepsilon(t,\boldsymbol{r}),\ \boldsymbol{r}\in\mathbb{R}^d,\ t\in\mathbb{R}, \tag{1.1}$$

where ψ^ε is the complex-valued wave function, $0<\varepsilon\ll 1$ is the dimensionless rescaled Planck constant, $U=U(x)$ is a smooth real-valued external potential function, and V_Γ is a (real) periodic potential function with linearly independent lattice vectors $\{\boldsymbol{v}_1,\boldsymbol{v}_2,...,\boldsymbol{v}_d\}\subset\mathbb{R}^d$, *i.e.*

$$V_\Gamma(\boldsymbol{r}+\boldsymbol{v}) = V_\Gamma(\boldsymbol{r}), \quad \text{for all } \boldsymbol{v}=\sum_{j=1}^d m_j\boldsymbol{v}_j,\ m_j\in\mathbb{Z}. \tag{1.2}$$

The lattice is then denoted by

$$\Gamma = \left\{\sum_{j=1}^d m_j\boldsymbol{v}_j\ ,\ m_j\in\mathbb{Z}\right\}, \tag{1.3}$$

and the fundamental domain of the lattice Γ is $\mathcal{C}=\left\{\sum_{j=1}^d x_j\boldsymbol{v}_j\ ,\ x_j\in[0,1]\right\}$. The reciprocal lattice Γ^* is generated by the vectors $\boldsymbol{k}_j$ for $1\le j\le d$ which are defined by $\boldsymbol{v}_i\cdot\boldsymbol{k}_j=2\pi\delta_{ij}$, where we denote the Kronecker delta by δ_{ij}. Then the first Brillouin zone is given by $B=\left\{\sum_{j=1}^d \xi_j\boldsymbol{k}_j\ ,\ \xi_j\in[-1/2,\,1/2]\right\}$.

The asymptotic behavior of the solution ψ^ε of (1.1) as $\varepsilon\to 0$ has been intensively studied. One of the most striking effects is that the electrons remain semiclassically in a certain quantum subsystem, "move along the m-th band" and the dynamics is given by $\dot{\boldsymbol{r}}=\partial_{\boldsymbol{k}}E_m(\boldsymbol{k})$, $\dot{\boldsymbol{k}}=-\partial_{\boldsymbol{r}}U$, where E_m is the energy corresponding to the m-th *Bloch band* [9], and U is the external potential. This result has been justified both from a physical point of view in, *e.g.* [4, 42], and from a mathematical point of view in, *e.g.* [30, 18, 6, 7]. Higher order corrections relevant to the Berry phase can be included, see *e.g.* [34, 35, 15]. One remark is that all of these results use the *adiabatic* assumption, namely different Bloch bands are well-separated and there is no band-crossing. Nevertheless the inter-band transition effect should be considered whenever the transitions between energy bands of the quantum system play an important role. This may happen when the gap between the energy bands becomes small

enough in comparison to the scaled Planck constant ε or at conical crossings where the bands intersect. The study of such "quantum tunnelings" is important in many applications, from quantum dynamics in chemical reaction [39], semiconductors to Bose-Einstein condensation [10]. Mathematical studies on band-crossings can be found in *e.g.* [20, 26, 29]. One of the most interesting applications of (1.1) is when Γ has a honeycomb lattice structure, which can be used to model the electronic behavior in a graphene layer. The Dirac equation has been used to study the electronic properties of graphene [33] and its connection with the Schrödinger equation has been studied in [2, 1]. The existence of the Dirac points in a honeycomb lattice and the convergence of the solution in the semiclassical limit have been proved in [16, 17], and in the weak nonlinear case in [3].

A review of mathematical and computational method of semiclassical Schrödinger equation can be found in [25]. The direct numerical simulation of (1.1) is usually very expensive due to the small parameter ε and the highly oscillating structure of V_Γ. The standard time-splitting spectral method [5] requires both the mesh size and the time step much smaller than ε. A Bloch decomposition-based time-splitting (BDTS) method [21, 22] can relax the time step requirement to be $O(1)$, which has a huge advantage in saving the computational time. However the BDTS still requires a mesh size of $O(\varepsilon)$, which is expensive especially for very small ε and higher dimensions. For the asymptotic methods, a modified WKB method based on Bloch decomposition was derived in [8], which leads to a system of eikonal and transport equations. An approximation by system of eikonal and transport equations can be derived using the Bloch decomposition and a modified WKB method. However the WKB approximation do not give a good accuracy around caustics. A Gaussian beam method based on the Bloch decomposition developed in [24] provides an efficient approximate method that allows an accurate solution to (1.1) around caustics. A common assumption of these approaches is that the Bloch bands are well separated. When band-crossing happens, the approximations cannot handle the inter-band transition effect. Different multi-band models have been developed in order to capture the inter-band transitions, *e.g.* [11, 32, 31]. In [13] the authors derived a semiclassical model for the Schrödinger equation with periodic potentials (1.1) that account for band-crossings using Wigner-Bloch theory and proposed a hybrid method for multiscale computation.

In this paper, we develop a new Bloch decomposition-based Gaussian beam (BDGB) approximation in the momentum space to solve the Schrödinger equation (1.1) away from the band-crossings. The BDGB method is derived in the momentum space by taking the

Bloch transformation to the Schrödinger equation, which is different from the physical space Gaussian beam method that was developed in [24]. To deal with the band-crossings (which happen in the momentum space), we couple the BDGB method with the BDTS method in a natural way: away from the band-crossing zone the BDGB method is applied, around the band-crossings the BDTS method is applied, and the exchange of data between different zones is achieved simply by Gaussian beam decomposition [38]. We also numerically investigate the Dirac approximation that Fefferman and Weinstein proposed in [16, 17]. By comparing the Schrödinger solutions and the Dirac solutions in different external potential cases, we show that the Dirac system is a good approximation only when the external potential is zero or small.

The rest of this paper is organized as follows: In Section 2 we recall in detail the Bloch transformation and decomposition in general d-dimensional space. Then in Section 3 we present the new BDGB method for the periodic Schrödinger equation. We also present an implementation of the BDTS method locally in the quasi-momentum space. In Section 4 we present the hybrid method coupling the BDGB method and BDTS method in details, and test the hybrid method numerically on the periodic Schrödinger equation with band-crossings. As an application we show simulation result of the Schrödinger equation with a honeycomb lattice potential in the two dimensional position space. In Section 5, we briefly review the Dirac approximation and numerically investigate it in presence of different external potentials.

2 The lattice potential and Bloch transformation

Given a lattice Γ, one can transform it to the standard square lattice by changing variables. Let

$$\boldsymbol{r} = \frac{1}{2\pi}\sum_{j=1}^{d} x_j \boldsymbol{v}_j = Q\boldsymbol{x}, \tag{2.1}$$

where Q is the matrix $[\boldsymbol{v}_1, \boldsymbol{v}_2, ..., \boldsymbol{v}_d]/(2\pi)$ and $\boldsymbol{x}$ is the vector $(x_1, x_2, ..., x_d)^T \in \mathbb{R}^d$. Then the gradient on $\boldsymbol{r}$ can be replaced by $\nabla_{\boldsymbol{r}} = \left(Q^{-1}\right)^T \nabla_{\boldsymbol{x}} = A\nabla_{\boldsymbol{x}}$, where $A = \left(Q^{-1}\right)^T = [\boldsymbol{k}_1, \boldsymbol{k}_2, ..., \boldsymbol{k}_d]$. Define $\tilde{\psi^\varepsilon}(\boldsymbol{x}) = \psi^\varepsilon(Q\boldsymbol{x})$, $\tilde{V}_\Gamma(\boldsymbol{x}) = V_\Gamma(Q\boldsymbol{x})$, and $\tilde{U}(\boldsymbol{x}) = U(Q\boldsymbol{x})$, then from (1.1) one gets

$$\mathrm{i}\varepsilon\partial_t\tilde{\psi^\varepsilon}(t,\boldsymbol{x}) = -\frac{\varepsilon^2}{2}\left(A\nabla_{\boldsymbol{x}}\right)^2\tilde{\psi^\varepsilon}(t,\boldsymbol{x}) + \left(\tilde{V}_\Gamma\left(\frac{\boldsymbol{x}}{\varepsilon}\right) + \tilde{U}(\boldsymbol{x})\right)\tilde{\psi^\varepsilon}(t,\boldsymbol{x}), \tag{2.2}$$

where $\tilde{V}_\Gamma$ is a periodic potential on the standard square lattice $\tilde{\Gamma}$ defined by the lattice vectors $\{\boldsymbol{e}_j = (2\pi\delta_{ij})_{i=1}^d,\ 1 \le j \le d\}$. For example in the two dimensional case, a typical example is the following honeycomb lattice potential [16, 17] (appears in the model of 2D graphene by the Dirac equation, with the vertices of the lattice corresponding to Dirac points)

$$V_\Gamma(\boldsymbol{r}) = \cos(\boldsymbol{k_1}\cdot\boldsymbol{r}) + \cos(\boldsymbol{k_2}\cdot\boldsymbol{r}) + \cos((\boldsymbol{k_1}+\boldsymbol{k_2})\cdot\boldsymbol{r}) + V_0, \tag{2.3}$$

and then corresponding lattice vectors are

$$\boldsymbol{v}_1 = \pi\begin{pmatrix}\sqrt{3}\\1\end{pmatrix}, \quad \boldsymbol{v}_2 = \pi\begin{pmatrix}\sqrt{3}\\-1\end{pmatrix}, \tag{2.4}$$

with the reciprocal lattice vectors as

$$\boldsymbol{k}_1 = \begin{pmatrix}1/\sqrt{3}\\1\end{pmatrix}, \quad \boldsymbol{k}_2 = \begin{pmatrix}1/\sqrt{3}\\-1\end{pmatrix}. \tag{2.5}$$

See Figures 2.1 and 2.2 for the lattice structures.

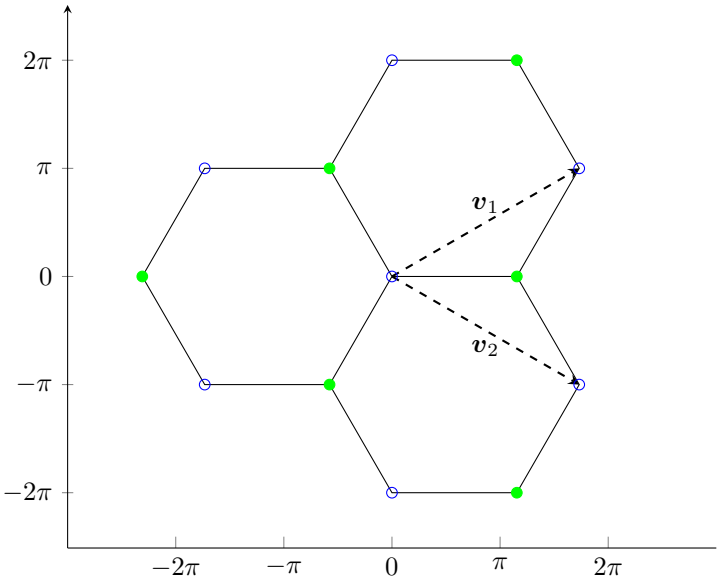

Figure 2.1: The honeycomb lattice structure

By taking the lattice transformation (2.1), (2.3) can be transformed to the standard square lattice potential:

$$\tilde{V}_\Gamma(\boldsymbol{x}) = \cos(x_1) + \cos(x_2) + \cos(x_1 + x_2) + V_0. \tag{2.6}$$

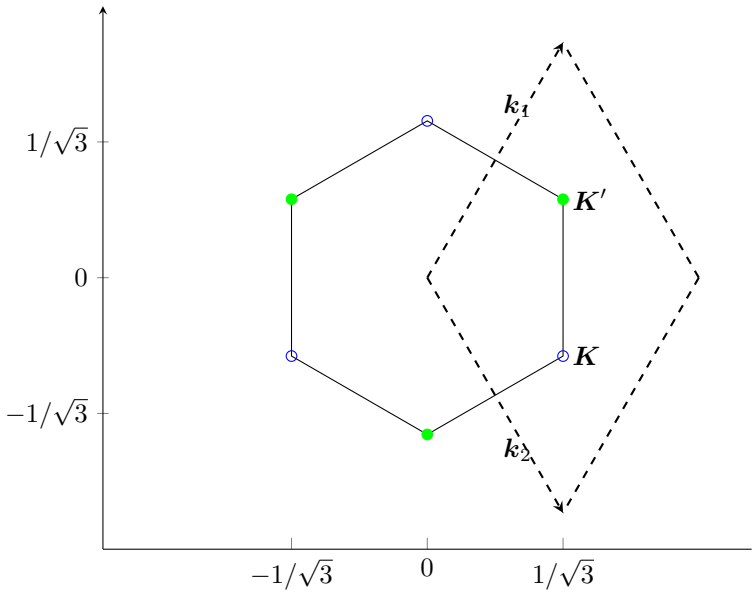

Figure 2.2: The reciprocal honeycomb lattice structure and the Dirac points

From now on we use ∇^A and $\left(\nabla^A\right)^2$ to denote $A\nabla$ and $\nabla^A \cdot \nabla^A$ respectively, and drop the tilde to get the Schrödinger equation with a periodic potential V_Γ in a standard square lattice $\Gamma = a\mathbb{Z}$:

$$\mathrm{i}\varepsilon\partial_t\psi^\varepsilon(t,\boldsymbol{x}) = -\frac{\varepsilon^2}{2}\left(\nabla^A\right)^2\psi^\varepsilon(t,\boldsymbol{x}) + \left(V_\Gamma\left(\frac{\boldsymbol{x}}{\varepsilon}\right) + U(\boldsymbol{x})\right)\psi^\varepsilon(t,\boldsymbol{x}). \tag{2.7}$$

Notice that the symbol for $\left(\nabla^A\right)^2$ is $|A\boldsymbol{\xi}|^2$, which guarantee that $\left(\nabla^A\right)^2$ is uniformly elliptic.

2.1 The Bloch decomposition

Let V_Γ be a periodic potential on the lattice $\Gamma = 2\pi\,\mathbb{Z}^d$, so $V_\Gamma(\boldsymbol{x}+\boldsymbol{\nu}) = V_\Gamma(\boldsymbol{x})$ for any $\boldsymbol{x} \in \mathbb{R}^d$ and $\boldsymbol{\nu} \in \Gamma$. We denote the dual lattice of Γ by Γ^* and $\Gamma^* = \mathbb{Z}^d$. The fundamental domain of Γ is $\mathcal{C} = [0, 2\pi]^d$ and the first Brillouin zone is $\mathcal{B} = \left[-\frac{1}{2}, \frac{1}{2}\right]^d$. Define $\{E_m(\boldsymbol{\xi}), \Psi_m(\boldsymbol{z},\boldsymbol{\xi})\}$ as the m-th eigen-pair of the following problem:

$$\begin{aligned} -\frac{1}{2}\left(\nabla_{\boldsymbol{z}}^A\right)^2\Psi_m(\boldsymbol{z},\boldsymbol{\xi}) + V_\Gamma(\boldsymbol{z})\Psi_m(\boldsymbol{z},\boldsymbol{\xi}) &= E_m(\boldsymbol{\xi})\Psi_m(\boldsymbol{z},\boldsymbol{\xi}), \\ \Psi_m(\boldsymbol{z}+\boldsymbol{\nu},\boldsymbol{\xi}) &= \mathrm{e}^{\mathrm{i}\boldsymbol{\xi}\cdot\boldsymbol{\nu}}\Psi_m(\boldsymbol{z},\boldsymbol{\xi}), \end{aligned} \tag{2.8}$$

for $\boldsymbol{z} \in \mathbb{R}^d$ and $\boldsymbol{\xi} \in \mathcal{B}$. We then call E_m the m-th Bloch band and Ψ_m the m-th Bloch function [9]. Define $\Phi_m(\boldsymbol{z},\boldsymbol{\xi}) = \mathrm{e}^{-\mathrm{i}\boldsymbol{\xi}\cdot\boldsymbol{z}}\Psi_m(\boldsymbol{z},\boldsymbol{\xi})$ as the periodic part of the Bloch function

Ψ_m one can show that Φ_m satisfies

$$\begin{aligned}\left(\frac{1}{2}\left(-\mathrm{i}\nabla_{\boldsymbol{z}}^{A}+\boldsymbol{\xi}\right)^{2}+V_{\Gamma}(\boldsymbol{z})\right)\Phi_m(\boldsymbol{z},\boldsymbol{\xi})&=E_m(\boldsymbol{\xi})\Phi(\boldsymbol{z},\boldsymbol{\xi}),\\ \Phi_m(\boldsymbol{z}+\boldsymbol{\nu},\boldsymbol{\xi})&=\Phi_m(\boldsymbol{z},\boldsymbol{\xi}).\end{aligned}\tag{2.9}$$

It has been shown in [40] that $\{E_m,\Psi_m\}_{m\in\mathbb{N}}$ have the following properties:

(a) The eigenvalues $E_m=E_m(\boldsymbol{\xi})$ are Lipschitz continuous and Γ^*-periodic in $\boldsymbol{\xi}$ and can be ordered according to $E_1(\boldsymbol{\xi})\le E_2(\boldsymbol{\xi})\le ...\le E_m(\boldsymbol{\xi})\le ...$ with $E_m\to\infty$ as $m\to\infty$.

(b) For any $\boldsymbol{\xi}\in\mathcal{B}$, $\{\Psi_m(\cdot,\boldsymbol{\xi})\}$ forms a complete orthonormal basis in $L^2(\mathcal{C})$, *i.e.*

$$\langle\Psi_m,\Psi_n\rangle:=\int_{\mathcal{C}}\Psi_m(\boldsymbol{z},\boldsymbol{\xi})\bar{\Psi}_n(\boldsymbol{z},\boldsymbol{\xi})\mathrm{d}\boldsymbol{z}=(2\pi)^d\delta_{mn}.\tag{2.10}$$

(c) For all $\phi\in L^2(\mathbb{R}^d)$, one has the following Bloch decomposition:

$$\phi(\boldsymbol{x})=\sum_{m}^{\infty}\int_{\mathcal{B}}c_m(\boldsymbol{\xi})\Psi_m(\boldsymbol{x},\boldsymbol{\xi})\,\mathrm{d}\boldsymbol{\xi}=\sum_{m}^{\infty}\int_{\mathcal{B}}\int_{\mathbb{R}^d}\phi(\boldsymbol{z})\bar{\Psi}_m(\boldsymbol{z},\boldsymbol{\xi})\Psi_m(\boldsymbol{x},\boldsymbol{\xi})\,\mathrm{d}\boldsymbol{x}\mathrm{d}\boldsymbol{\xi}.\tag{2.11}$$

(d) The d-dimensional Lebesgue measure of the band-crossing set $\{\boldsymbol{\xi}\in\bar{\mathcal{B}}:E_n(\boldsymbol{\xi})=E_m(\boldsymbol{\xi}),\,n\neq m\}$ is zero.

For example, in Figure 2.3, we plot the first eighth bands for $V_\Gamma(x)=\cos(x)$ in the 1D case. One can see that some of the band gaps are very small around $\xi=0,\pm0.5$, *e.g.* , the minimal band gap between E_6 and E_7 is around 6.76×10^{-5}. In Figure 2.4 we plot the first two bands for $V_\Gamma(x_1,x_2))=\cos(x_1)+\cos(x_2)+\cos(x_1+x_2)$ in the 2D case at $\boldsymbol{\xi}=(2/3,1/3)$ and $\boldsymbol{\xi}=(1/3,2/3)$. Actually, it has been proven in [16] that the first two bands for $V_\Gamma(x_1,x_2)=\cos(x_1)+\cos(x_2)+\cos(x_1+x_2)$ feature two conical crossings (at the Dirac points) in the first Brillouin zone.

2.2 The Schrödinger equation under the Bloch transformation

To consider the Schrödinger equation in the quasi-momentum space, we introduce a new function $\tilde{\psi^\varepsilon}$ by taking the Bloch transformation [35, 21] $\mathcal{T}$ of the wave function ψ^ε as

$$\tilde{\psi^\varepsilon}(\boldsymbol{y},\boldsymbol{\xi})=\left(\mathcal{T}\psi^\varepsilon\right)(\boldsymbol{y},\boldsymbol{\xi})=\sum_{\boldsymbol{\gamma}\in\Gamma}\mathrm{e}^{-\mathrm{i}\boldsymbol{\gamma}\cdot\boldsymbol{\xi}}\psi^\varepsilon\left(\varepsilon(\boldsymbol{y}+\boldsymbol{\gamma})\right).\tag{2.12}$$

It is easy to see that $\tilde{\psi^\varepsilon}$ is quasi-periodic with respect to $\boldsymbol{y}$ and periodic with respect to $\boldsymbol{\xi}$, *i.e.* ,

$$\tilde{\psi^\varepsilon}(\boldsymbol{y}+\boldsymbol{\gamma},\boldsymbol{\xi})=\tilde{\psi^\varepsilon}(\boldsymbol{y},\boldsymbol{\xi})\mathrm{e}^{\mathrm{i}\boldsymbol{\gamma}\cdot\boldsymbol{\xi}},\quad\forall\boldsymbol{\gamma}\in\Gamma,\tag{2.13}$$

$$\tilde{\psi^\varepsilon}(\boldsymbol{y},\boldsymbol{\xi}+\boldsymbol{\nu})=\tilde{\psi^\varepsilon}(\boldsymbol{y},\boldsymbol{\xi}),\qquad\forall\boldsymbol{\nu}\in\Gamma^*.\tag{2.14}$$

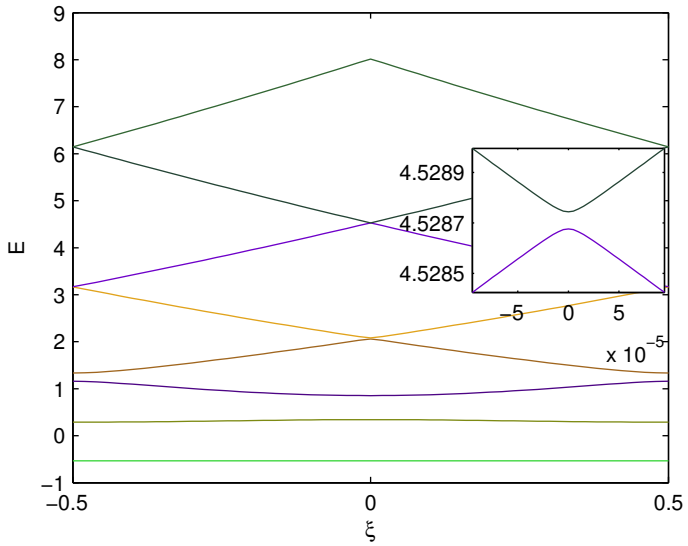

Figure 2.3: The first eight Bloch bands for $V_\Gamma(x) = \cos(x)$. The zoom in figure plots the 6-th and 7-th band in the tiny neighborhood of $\xi = 0$.

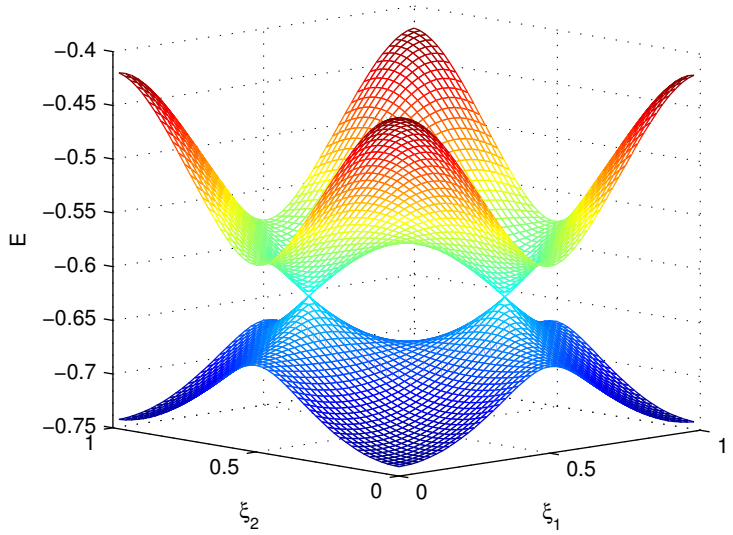

Figure 2.4: The first two Bloch bands for $V_\Gamma(x_1, x_2) = \cos(x_1) + \cos(x_2) + \cos(x_1 + x_2)$.

Notice that it satisfies

$$\int_{\mathcal{B}} \tilde{\psi}^{\varepsilon}\left(\frac{\boldsymbol{x}}{\varepsilon}, \boldsymbol{\xi}\right) \mathrm{d}\boldsymbol{\xi} = \int_{\mathcal{B}} \sum_{\boldsymbol{\gamma}\in\Gamma} \mathrm{e}^{-\mathrm{i}\boldsymbol{\gamma}\cdot\boldsymbol{\xi}} \psi^{\varepsilon}\left(\boldsymbol{x}+\varepsilon\boldsymbol{\gamma}\right) \mathrm{d}\boldsymbol{\xi} = \sum_{\boldsymbol{\gamma}\in\Gamma} \delta_{\boldsymbol{\gamma}\mathbf{0}} \psi^{\varepsilon}\left(\boldsymbol{x}+\varepsilon\boldsymbol{\gamma}\right) = \psi^{\varepsilon}(\boldsymbol{x}),$$

so it is natural to define the inverse Bloch transformation $\mathcal{T}^{-1}$ by

$$(\mathcal{T}^{-1}\tilde{\psi}^{\varepsilon})(\boldsymbol{x}) = \int_{\mathcal{B}} \tilde{\psi}^{\varepsilon}\left(\frac{\boldsymbol{x}}{\varepsilon}, \boldsymbol{\xi}\right) \mathrm{d}\boldsymbol{\xi} = \int_{\mathcal{B}} \tilde{\psi}^{\varepsilon}\left(\boldsymbol{y}, \boldsymbol{\xi}\right) \mathrm{d}\boldsymbol{\xi}\Big|_{\boldsymbol{y}=\frac{\boldsymbol{x}}{\varepsilon}}. \tag{2.15}$$

It is easy to find the following pseudo-differential relations:

$$\begin{aligned} \mathcal{T}(-\mathrm{i}\varepsilon\nabla_{\boldsymbol{x}})\mathcal{T}^{-1} &= -\mathrm{i}\nabla_{\boldsymbol{y}}, \\ \mathcal{T}\,\boldsymbol{x}\,\mathcal{T}^{-1} &= \mathrm{i}\varepsilon\nabla_{\boldsymbol{\xi}} + \varepsilon\boldsymbol{y}, \\ \mathcal{T}V_{\Gamma}(\boldsymbol{x}/\varepsilon)\mathcal{T}^{-1} &= V_{\Gamma}(\boldsymbol{y}). \end{aligned} \tag{2.16}$$

Actually one can verify them by a formal calculation as follows,

$$\begin{aligned} \mathcal{T}(-\mathrm{i}\varepsilon\nabla_{\boldsymbol{x}})\mathcal{T}^{-1}\tilde{\psi}^{\varepsilon}(\boldsymbol{y},\boldsymbol{\xi}) &= \left(\mathcal{T}(-\mathrm{i}\varepsilon\nabla_{\boldsymbol{x}}) \int_{\mathcal{B}} \tilde{\psi}^{\varepsilon}\left(\frac{\boldsymbol{x}}{\varepsilon}, \boldsymbol{\xi}\right) \mathrm{d}\boldsymbol{\xi}\right)(\boldsymbol{y},\boldsymbol{\xi}) \\ &= \left(\mathcal{T}\int_{\mathcal{B}} (-\mathrm{i}\nabla_{\boldsymbol{y}})\tilde{\psi}^{\varepsilon}\left(\boldsymbol{y},\boldsymbol{\xi}\right) \mathrm{d}\boldsymbol{\xi}\Big|_{\boldsymbol{y}=\frac{\boldsymbol{x}}{\varepsilon}}\right)(\boldsymbol{y},\boldsymbol{\xi}) \\ &= \mathcal{T}\mathcal{T}^{-1}(-\mathrm{i}\nabla_{\boldsymbol{y}}\tilde{\psi}^{\varepsilon}(\boldsymbol{y},\boldsymbol{\xi})) = -\mathrm{i}\nabla_{\boldsymbol{y}}\tilde{\psi}^{\varepsilon}(\boldsymbol{y},\boldsymbol{\xi}); \end{aligned}$$

$$\begin{aligned} \mathcal{T}x\mathcal{T}^{-1}\tilde{\psi}^{\varepsilon}(\boldsymbol{y},\boldsymbol{\xi}) &= \left(\mathcal{T}x \int_{\mathcal{B}} \tilde{\psi}^{\varepsilon}\left(\frac{\boldsymbol{x}}{\varepsilon}, \boldsymbol{\xi}\right) \mathrm{d}\boldsymbol{\xi}\right)(\boldsymbol{y},\boldsymbol{\xi}) \\ &= \sum_{\boldsymbol{\gamma}\in\Gamma} \mathrm{e}^{-\mathrm{i}\boldsymbol{\gamma}\cdot\boldsymbol{\xi}}\varepsilon(\boldsymbol{y}+\boldsymbol{\gamma}) \int_{\mathcal{B}} \tilde{\psi}^{\varepsilon}\left(\boldsymbol{y}+\boldsymbol{\gamma},\boldsymbol{\xi}'\right) \mathrm{d}\boldsymbol{\xi}' \\ &= \sum_{\boldsymbol{\gamma}\in\Gamma} \varepsilon(\boldsymbol{y}+\boldsymbol{\gamma}) \int_{\mathcal{B}} \tilde{\psi}^{\varepsilon}\left(\boldsymbol{y},\boldsymbol{\xi}'\right) \mathrm{e}^{-\mathrm{i}\boldsymbol{\gamma}\cdot(\boldsymbol{\xi}-\boldsymbol{\xi}')} \mathrm{d}\boldsymbol{\xi}' \\ &= \varepsilon\boldsymbol{y}\tilde{\psi}^{\varepsilon}(\boldsymbol{y},\boldsymbol{\xi}) + \varepsilon \sum_{\boldsymbol{\gamma}\in\Gamma} \int_{\mathcal{B}} \boldsymbol{\gamma}\tilde{\psi}^{\varepsilon}\left(\boldsymbol{y},\boldsymbol{\xi}'\right) \mathrm{e}^{-\mathrm{i}\boldsymbol{\gamma}\cdot(\boldsymbol{\xi}-\boldsymbol{\xi}')} \mathrm{d}\boldsymbol{\xi}' \\ &= (\mathrm{i}\varepsilon\nabla_{\boldsymbol{\xi}} + \varepsilon\boldsymbol{y})\,\tilde{\psi}^{\varepsilon}(\boldsymbol{y},\boldsymbol{\xi}). \end{aligned}$$

Now let us apply $\mathcal{T}(\cdot)\mathcal{T}^{-1}$ to the Schrödinger equation (2.7) and obtain an equation for $\tilde{\psi}^{\varepsilon}$

$$\mathrm{i}\varepsilon\partial_t\tilde{\psi}^{\varepsilon}(t,\boldsymbol{y},\boldsymbol{\xi}) = \left(-\frac{1}{2}\left(\nabla_{\boldsymbol{y}}^{A}\right)^2 + V_{\Gamma}(\boldsymbol{y})\right)\psi^{\varepsilon}(t,\boldsymbol{y},\boldsymbol{\xi}) + U\left(\mathrm{i}\varepsilon\nabla_{\boldsymbol{\xi}} + \varepsilon\boldsymbol{y}\right)\psi^{\varepsilon}(t,\boldsymbol{y},\boldsymbol{\xi}), \tag{2.17}$$

where we use the pseudo-differential operator $U\left(\mathrm{i}\varepsilon\nabla_{\boldsymbol{\xi}} + \varepsilon\boldsymbol{y}\right)$ to denote $\mathcal{T}U(\boldsymbol{x})\mathcal{T}^{-1}$.

Since for every $\boldsymbol{\xi} \in \mathcal{B}$, the Bloch functions $\{\Psi_m(\cdot,\boldsymbol{\xi})\}_{m=1}^{\infty}$ form an orthonormal basis of $L^2(\mathcal{C})$, the solution of (2.17) can be decomposed as

$$\tilde{\psi}^{\varepsilon}(t,\boldsymbol{y},\boldsymbol{\xi}) = \sum_m \tilde{\psi}_m^{\varepsilon} = \sum_m c_m(t,\boldsymbol{\xi})\Psi_m(\boldsymbol{y},\boldsymbol{\xi}), \tag{2.18}$$

with the Bloch coefficient

$$c_m(t,\boldsymbol{\xi}) = \int_{\mathcal{C}} \tilde{\psi^\varepsilon}(t,\boldsymbol{y},\boldsymbol{\xi})\bar{\Psi}_m(\boldsymbol{y},\boldsymbol{\xi})\,\mathrm{d}\boldsymbol{y}. \tag{2.19}$$

Then by taking inner product of (2.17) w.r.t Ψ_n, one obtains the equation for c_n in the momentum space

$$\begin{aligned}\mathrm{i}\varepsilon\partial_t c_n(t,\boldsymbol{\xi}) &= E_n(\boldsymbol{\xi})c_n(t,\boldsymbol{\xi}) + \sum_m \int_{\mathcal{C}} \left(U\left(\mathrm{i}\varepsilon\nabla_{\boldsymbol{\xi}} + \varepsilon\boldsymbol{y}\right) c_m(t,\boldsymbol{\xi})\Psi_m(\boldsymbol{y},\boldsymbol{\xi})\right)\bar{\Psi}_n(\boldsymbol{y},\boldsymbol{\xi})\,\mathrm{d}\boldsymbol{y} \\ &= E_n(\boldsymbol{\xi})c_n(t,\boldsymbol{\xi}) + U\left(\mathrm{i}\varepsilon\nabla_{\boldsymbol{\xi}} + \varepsilon\boldsymbol{y}\right) c_n(t,\boldsymbol{\xi}) + \sum_m \mathcal{R}_{nm}c_m(t,\boldsymbol{\xi}),\end{aligned} \tag{2.20}$$

where the last term represents the band coupling:

$$\mathcal{R}_{nm}c_m(\boldsymbol{\xi}) = \int_{\mathcal{C}} \left(U\left(\mathrm{i}\varepsilon\nabla_{\boldsymbol{\xi}} + \varepsilon\boldsymbol{y}\right) c_m(\boldsymbol{\xi})\Psi_m(\boldsymbol{y},\boldsymbol{\xi})\right)\bar{\Psi}_n(\boldsymbol{y},\boldsymbol{\xi})\,\mathrm{d}\boldsymbol{y} - U\left(\mathrm{i}\varepsilon\nabla_{\boldsymbol{\xi}} + \varepsilon\boldsymbol{y}\right) c_m(\boldsymbol{\xi})\delta_{mn}.$$

Formally when U is smooth, the terms $\mathcal{R}_{nm}c_m$ are small ($= O(\varepsilon)$), so by ignoring them, one finds the decoupled equations

$$\mathrm{i}\varepsilon\partial_t c_n(t,\boldsymbol{\xi}) = E_n(\boldsymbol{\xi})c_n(t,\boldsymbol{\xi}) + U\left(\mathrm{i}\varepsilon\nabla_{\boldsymbol{\xi}} + \varepsilon\boldsymbol{y}\right) c_n(t,\boldsymbol{\xi}). \tag{2.21}$$

Actually it has been proved rigorously in [12, 34, 19], using different analytical approaches, that when the bands are well-separated and U is smooth, (2.21) gives ψ^ε as an $O(\varepsilon)$ approximation solution of (1.1).

3 Bloch decomposition-based methods

In this section, we propose a Bloch decomposition-based Gaussian Beam method in the momentum space in order to solve the periodic Schrödinger equation (1.1) in the semiclassical regime efficiently. We also review the Bloch decomposition-based time splitting method and adapt it to a local direct solver for (1.1).

3.1 The Bloch decomposition-based Gaussian beam method

The approximation. If initially the Bloch coefficient $c_m(0,\boldsymbol{\xi})$ has a Gaussian beam decomposition (*e.g.* [38])

$$\begin{aligned}c_m(0,\boldsymbol{\xi}) &= \sum_{g_m\in\mathcal{G}_m} a_m^0 \exp\left(-\frac{\mathrm{i}}{\varepsilon}T_m^0(\boldsymbol{\xi})\right) \\ &= \sum_{g_m\in\mathcal{G}_m} a_m^0 \exp\left(-\frac{\mathrm{i}}{\varepsilon}(S_m^0 + \boldsymbol{x}_m^0\cdot(\boldsymbol{\xi}-\boldsymbol{p}_m^0) + \frac{1}{2}M_m^0:(\boldsymbol{\xi}-\boldsymbol{p}_m^2)^2)\right),\end{aligned} \tag{3.1}$$

where $g_m = \{\boldsymbol{p}_m^0, \boldsymbol{x}_m^0, S_m^0, M_m^0, a_m^0\}$ denotes the beam parameter factor and $\mathcal{G}_m$ denotes the set of beam parameters g_m. We seek a Bloch decomposition-based Gaussian beam (BDGB) approximation to (2.17). Assume that the solution of (2.17) can be represented by a Gaussian beam ansatz:

$$\tilde{\psi}_m^\varepsilon(t, \boldsymbol{y}, \boldsymbol{\xi}) = a_m(t) \exp\left(-\frac{\mathrm{i}}{\varepsilon} T_m(t, \boldsymbol{\xi})\right) \Psi_m(\boldsymbol{y}, \boldsymbol{\xi}), \tag{3.2a}$$

$$T_m(t, \boldsymbol{\xi}) = S_m(t) + \boldsymbol{x}_m(t) \cdot (\boldsymbol{\xi} - \boldsymbol{p}_m(t)) + \frac{1}{2} M_m(t) : (\boldsymbol{\xi} - \boldsymbol{p}_m(t))^2 + O((\boldsymbol{\xi} - \boldsymbol{p}_m(t))^3), \tag{3.2b}$$

where Ψ_m is the m-th Bloch function, $\boldsymbol{p}_m$, $\boldsymbol{x}_m, \in \mathbb{R}^2$, $S_m \in \mathbb{R}$ and $M_m \in \mathbb{C}^{2\times 2}$. The imaginary part of M_m will be chosen as negative definite, *i.e.* , all the eigenvalues of $\mathrm{Im} M_m$ are positive.

Remark 3.1. The Gaussian ansatz we used in (3.2) is defined in the momentum space, and in (3.2a) the Bloch function factor Ψ_m does not depend on time t. So essentially we are working on a Gaussian beam approximation of the Bloch coefficient c_m defined in (2.18) and (2.19). This approach is different from that in [24], where a Gaussian beam ansatz in the position space was used and the Bloch function evolves with the beam propagation. Later in Section 4 we will see the approach (3.2) is convenient when coupled with the Bloch decomposition-based time splitting method locally around the band-crossings in the momentum space.

By defining $\tilde{\varphi}_m^\varepsilon = a_m \exp\left(-\mathrm{i} T_m/\varepsilon\right) \Phi_m$, where Φ_m is the periodic part of the Bloch function Ψ_m, *i.e.* $\Psi_m(\boldsymbol{y}, \boldsymbol{\xi}) = \exp(\mathrm{i}\boldsymbol{y} \cdot \boldsymbol{\xi}) \Phi_m(\boldsymbol{y}, \boldsymbol{\xi})$, the operator $(\mathrm{i}\nabla_{\boldsymbol{\xi}} + \boldsymbol{y})$ acting on $\tilde{\psi}_m^\varepsilon$ can be written as

$$(\mathrm{i}\varepsilon\nabla_{\boldsymbol{\xi}} + \varepsilon\boldsymbol{y})\tilde{\psi}_m^\varepsilon(\boldsymbol{y}, \boldsymbol{\xi}) = \exp(\mathrm{i}\boldsymbol{y} \cdot \boldsymbol{\xi})\, \mathrm{i}\varepsilon\nabla_{\boldsymbol{\xi}} \tilde{\varphi}_m^\varepsilon(\boldsymbol{y}, \boldsymbol{\xi}). \tag{3.3}$$

From (3.2) one can compute:

$$\begin{aligned}
\mathrm{i}\varepsilon\partial_t \tilde{\psi}_m^\varepsilon &= \left(\mathrm{i}\varepsilon \frac{\mathrm{d}a_m}{\mathrm{d}t} + a_m \partial_t T_m\right) \Psi_m \mathrm{e}^{-\mathrm{i}T_m/\varepsilon}, \\
\mathrm{i}\varepsilon\nabla_{\boldsymbol{\xi}} \tilde{\varphi}_m^\varepsilon &= a_m \left(\mathrm{i}\varepsilon\nabla_{\boldsymbol{\xi}} \Phi_m + \nabla_{\boldsymbol{\xi}} T_m \Phi_m\right) \mathrm{e}^{-\mathrm{i}T_m/\varepsilon}, \\
(\mathrm{i}\varepsilon\nabla_{\boldsymbol{\xi}})^2 \tilde{\varphi}_m^\varepsilon &= a_m \big((\nabla_{\boldsymbol{\xi}} T_m)^2 \Phi + \mathrm{i}\varepsilon\nabla_{\boldsymbol{\xi}}^2 T_m \Phi_m - \varepsilon^2 \nabla_{\boldsymbol{\xi}}^2 \Phi_m \\
&\qquad + \mathrm{i}\varepsilon(\nabla_{\boldsymbol{\xi}} T_m \wedge \nabla_{\boldsymbol{\xi}} \Phi_m + \nabla_{\boldsymbol{\xi}} \Phi_m \wedge \nabla_{\boldsymbol{\xi}} T_m)\big) \mathrm{e}^{-\mathrm{i}T_m/\varepsilon}.
\end{aligned} \tag{3.4}$$

Doing Taylor expansion of $U\left(\mathrm{i}\varepsilon\nabla_{\boldsymbol{\xi}}\right)$ at $\boldsymbol{x}_m$ up to 2nd order, one finds

$$\begin{aligned} U\left(\mathrm{i}\varepsilon\nabla_{\boldsymbol{\xi}}\right) \approx & U(\boldsymbol{x}_m) + \nabla_{\boldsymbol{x}} U(\boldsymbol{x}_m)\cdot\left(\mathrm{i}\varepsilon\nabla_{\boldsymbol{\xi}} - \boldsymbol{x}_m\right) + \frac{1}{2}\nabla_{\boldsymbol{x}}^2 U(\boldsymbol{x}_m) : \left(\mathrm{i}\varepsilon\nabla_{\boldsymbol{\xi}} - \boldsymbol{x}_m\right)^2 \\ = & U - \nabla_{\boldsymbol{x}} U\cdot\boldsymbol{x}_m + \frac{1}{2}\nabla_{\boldsymbol{x}}^2 U : \boldsymbol{x}_m^2 + \left(\nabla_{\boldsymbol{x}} U - \nabla_{\boldsymbol{x}}^2 U\cdot\boldsymbol{x}_m\right)\cdot\mathrm{i}\varepsilon\nabla_{\boldsymbol{\xi}} + \frac{1}{2}\nabla_{\boldsymbol{x}}^2 U : \left(\mathrm{i}\varepsilon\nabla_{\boldsymbol{\xi}}\right)^2. \end{aligned} \tag{3.5}$$

Plugging (3.4) and (3.5) into (2.17), matching the same order of ε, one obtains the $O(1)$ terms

$$\begin{aligned} \frac{\mathrm{d}}{\mathrm{d}t}T_m = & E_m + U - \nabla_{\boldsymbol{x}} U\cdot\boldsymbol{x}_m + \frac{1}{2}\nabla_{\boldsymbol{x}}^2 U : \boldsymbol{x}_m^2 \\ & + \left(\nabla_{\boldsymbol{x}} U - \nabla_{\boldsymbol{x}}^2 U\cdot\boldsymbol{x}_m\right)\cdot\nabla_{\boldsymbol{\xi}} T_m + \frac{1}{2}\nabla_{\boldsymbol{x}}^2 U : \left(\nabla_{\boldsymbol{\xi}} T_m\right)^2, \end{aligned} \tag{3.6}$$

and the $O(\varepsilon)$ terms

$$\begin{aligned} \frac{\mathrm{d}a_m}{\mathrm{d}t}\Phi_m = & a_m\left(\nabla_{\boldsymbol{x}} U - \nabla_{\boldsymbol{x}}^2 U\cdot\boldsymbol{x}_m\right)\cdot\nabla_{\boldsymbol{\xi}}\Phi_m + \frac{1}{2}a_m\nabla_{\boldsymbol{x}}^2 U : \nabla_{\boldsymbol{\xi}}^2 T_m\Phi_m \\ & + \frac{1}{2}a_m\nabla_{\boldsymbol{x}}^2 U : \left(\nabla_{\boldsymbol{\xi}} T_m\wedge\nabla_{\boldsymbol{\xi}}\Phi_m + \nabla_{\boldsymbol{\xi}}\Phi_m\wedge\nabla_{\boldsymbol{\xi}} T_m\right). \end{aligned} \tag{3.7}$$

Taking derivatives w.r.t ξ to (3.6) gives

$$\frac{\mathrm{d}}{\mathrm{d}t}\nabla_{\boldsymbol{\xi}} T_m = \nabla_{\boldsymbol{\xi}} E_m + \left(\nabla_{\boldsymbol{x}} U - \nabla_{\boldsymbol{x}}^2 U\cdot\boldsymbol{x}_m\right)\cdot\nabla_{\boldsymbol{\xi}}^2 T_m + \nabla_{\boldsymbol{\xi}}^2 T_m\,\nabla_{\boldsymbol{x}}^2 U\,\nabla_{\boldsymbol{\xi}} T_m, \tag{3.8}$$

$$\frac{\mathrm{d}}{\mathrm{d}t}\nabla_{\boldsymbol{\xi}}^2 T_m = \nabla_{\boldsymbol{\xi}}^2 E_m + \left(\nabla_{\boldsymbol{x}} U - \nabla_{\boldsymbol{x}}^2 U\cdot\boldsymbol{x}_m\right)\cdot\nabla_{\boldsymbol{\xi}}^3 T_m + \nabla_{\boldsymbol{\xi}}^2 T_m\,\nabla_{\boldsymbol{x}}^2 U\,\nabla_{\boldsymbol{\xi}}^2 T_m + \nabla_{\boldsymbol{\xi}}^3 T_m\,\nabla_{\boldsymbol{x}}^2 U\,\nabla_{\boldsymbol{\xi}} T_m. \tag{3.9}$$

By evaluating (3.6) – (3.9) at $\boldsymbol{\xi} = \boldsymbol{p}_m$ and using $\frac{\mathrm{d}\boldsymbol{p}_m}{\mathrm{d}t} = -\nabla_{\boldsymbol{x}} U$, we have

$$\frac{\mathrm{d}\boldsymbol{p}_m}{\mathrm{d}t} = -\nabla_{\boldsymbol{x}} U, \tag{3.10a}$$

$$\frac{\mathrm{d}\boldsymbol{x}_m}{\mathrm{d}t} = \nabla_{\boldsymbol{\xi}} E_m, \tag{3.10b}$$

$$\frac{\mathrm{d}S_m}{\mathrm{d}t} = E_m + U_m - \nabla_{\boldsymbol{x}} U_m\cdot\boldsymbol{x}_m, \tag{3.10c}$$

$$\frac{\mathrm{d}M_m}{\mathrm{d}t} = \nabla_{\boldsymbol{\xi}}^2 E_m + M_m\,\nabla_{\boldsymbol{x}}^2 U\,M_m, \tag{3.10d}$$

$$\frac{\mathrm{d}a_m}{\mathrm{d}t} = \nabla_{\boldsymbol{x}} U\cdot\left\langle\nabla_{\boldsymbol{\xi}}\Phi_m, \Phi_m\right\rangle a_m + \frac{1}{2}\nabla_{\boldsymbol{x}}^2 U : M_m\,a_m. \tag{3.10e}$$

Note that in (3.10e) $\mathcal{A}_m = \left\langle\nabla_{\boldsymbol{\xi}}\Phi_m, \Phi_m\right\rangle$ is the so-called Berry-connection [12, 35]. Notice that we have gauge freedom in choosing Bloch functions, *i.e.* , for any real function $\theta(\boldsymbol{\xi})$, $\mathrm{e}^{i\theta(\boldsymbol{\xi})}\Psi_m$ also provides a set of Bloch functions. In general this make it is difficult in numerical to select the smooth phase dependent Bloch waves, such that the gradient in the Berry-connection make sense. We remark here that for the numerical examples we proposed in

this paper, the smooth Bloch waves are selected in advance. On the other hand, we refer to [14] for a technique in getting the gauge invariant approximation of (3.10e).

The equations (3.10a)-(3.10b) are the ray-tracing equations, (3.10d) is a Riccati equation for the Hessian M_m, which can be solved by the dynamic first order system of ray tracing equations

$$\frac{\mathrm{d}P_m}{\mathrm{d}t} = -\nabla_{\boldsymbol{x}}^2 U\, R_m, \quad \frac{\mathrm{d}R_m}{\mathrm{d}t} = \nabla_{\boldsymbol{\xi}}^2 E_m\, P_m, \tag{3.11}$$

$$M_m = R_m P_m^{-1}. \tag{3.12}$$

Then, we can solve (3.10) with initial conditions

$$\begin{aligned} &\boldsymbol{p}_m(0,g_m) = \boldsymbol{p}_m^0,\ \boldsymbol{x}_m(0,g_m) = \boldsymbol{x}_m^0,\ S_m(0,g_m) = S_m^0, \\ &M_m(0,g_m) = M_m^0,\ a_m(0,g_m) = a_m^0, \end{aligned} \tag{3.13}$$

where the beam parameter $g_m = \{\boldsymbol{p}_m^0, \boldsymbol{x}_m^0, S_m^0, M_m^0, a_m^0\}$ comes from the initial decomposition (3.1), and compute the solutions $a_m(t,g_m)$, and

$$T_m(t,\boldsymbol{\xi},g_m) = S_m(t,g_m) + \boldsymbol{x}_m(t,g_m)\cdot(\boldsymbol{\xi} - \boldsymbol{p}_m(t,g_m)) + \frac{1}{2}M_m(t,g_m) : (\boldsymbol{\xi} - \boldsymbol{p}_m(t,g_m))^2.$$

Then the wave function $\tilde{\psi}^\varepsilon$ can be approximated by ${\tilde{\psi}^\varepsilon}_{GB}$ reconstructed from the beam summation

$${\tilde{\psi}^\varepsilon}_{GB}(t,\boldsymbol{y},\boldsymbol{\xi}) = \sum_{m=1}^{\infty}\sum_{g_m\in\mathcal{G}_m} a_m(t,g_m)\exp\left(-\frac{\mathrm{i}}{\varepsilon}T_m(t,\boldsymbol{\xi},g_m)\right)\Psi_m(\boldsymbol{y},\boldsymbol{\xi}). \tag{3.14}$$

A numerical test. In order to test the accuracy of the Bloch decomposition-based Gaussian beam method, we take one example in 1D for the periodic potential $V_\Gamma(x) = \cos(x)$. The initial data is chosen as

$$\begin{aligned} &\psi_0^\varepsilon(x) = a_0(x)\mathrm{e}^{\frac{\mathrm{i}}{\varepsilon}\xi_0 x}, \quad \text{with } \xi_0 = -1/4, \\ &a_0(x) = \left(\frac{8}{\varepsilon\pi}\right)^{\frac{1}{4}}\exp\left(-\frac{4(x-\pi)^2}{\varepsilon}\right), \end{aligned} \tag{3.15}$$

and the external potential is chosen as the harmonic potential $U(x) = \frac{1}{2}(x-\pi)^2$. We solve the Schrödinger equation (2.7) up to time $t = 1/4$ using the BDGB method and compare the result with the "exact" solution which is computed using the Bloch decomposition-based time splitting (BDTS) method with the mesh size and time step chosen small enough.

In Table 3.1, we show the L^2-errors between the Schrödinger solution ψ^ε and the Gaussian beam solution ψ_{GB}^ε. The convergence rate in ε is about of order 0.5. In Figure 3.1 we plot the densities and the absolute errors for different ε.

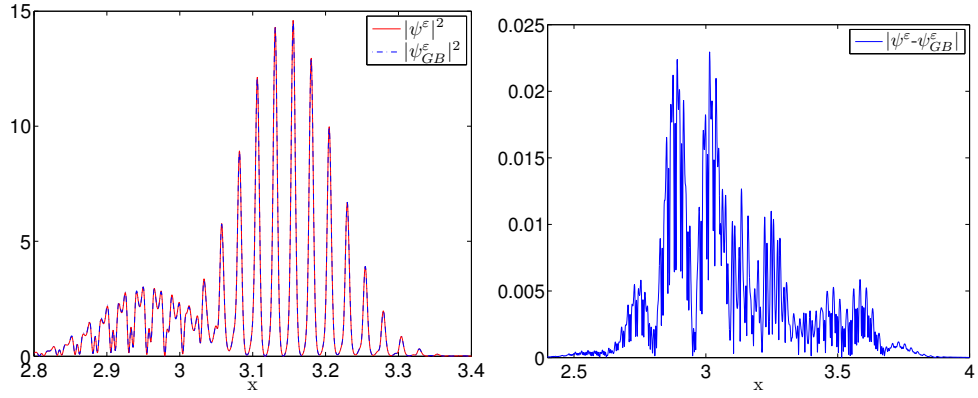

(a) $\varepsilon = 2^{-8}$

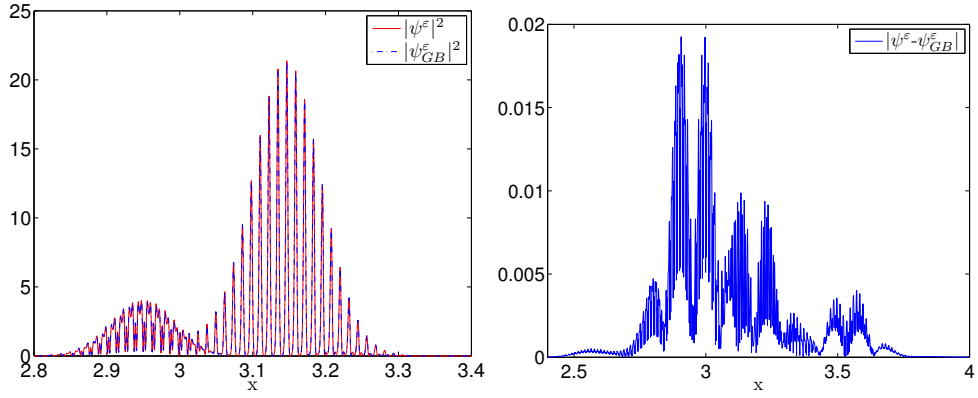

(b) $\varepsilon = 2^{-9}$

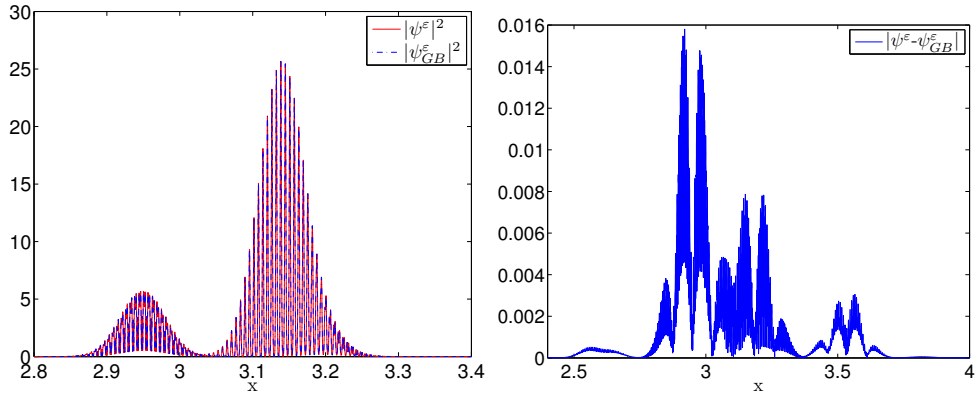

(c) $\varepsilon = 2^{-10}$

Figure 3.1: The Schrödinger solution versus the Gaussian beam solution at $t = 1/4$. Left column: the comparisons of the density at time $t = 1/4$; right column: the absolute value of difference between the Schrödinger solution and the Gaussian beam solution.

Table 3.1: The L^2-errors of wave function for the BDGB method at $t = 1/4$.

ε	2^{-7}	2^{-8}	2^{-9}	2^{-10}
$\|\psi^\varepsilon - \psi^\varepsilon_{GB}\|_2$	1.12E-2	7.42E-3	5.33E-3	3.66E-3

The Gaussian beam method requires the solution of a system of ODEs, and the number of ODEs is usually $O(1/\varepsilon^{d/2})$ where d is the dimension. Thus it is more efficient when $\varepsilon \ll 1$ in comparison with the direct solver like the Bloch decomposition-based time splitting method which requires $O(1/\varepsilon^d)$ mesh grids. From (3.2) we see the Gaussian beams are defined along the Bloch bands, and there is not any exchange between different bands, so the BDGB method is actually a semiclassical approximation under the adiabatic assumption, *i.e.* no inter-band transition happens. But when the band gap is small or even when band-crossing happens, the inter-band transitions become significant and cannot be ignored, and thus the BDGB approximation is not an accurate approach.

3.2 The Bloch decomposition-based time splitting method

In this section, the Bloch decomposition-based time splitting (BDTS) method [21, 22] is briefly reviewed. In particular we implement this method locally in the momentum space. The BDTS method solves the Schrödinger equation (2.7) in two steps, one for the free periodic Schrödinger equation and the other for the external potential part.

Step 1. Solve the free Schrödinger equation with periodic potential

$$\mathrm{i}\varepsilon\partial_t\psi^\varepsilon(t,\boldsymbol{x}) = -\frac{\varepsilon^2}{2}\left(\nabla^A\right)^2\psi^\varepsilon(t,\boldsymbol{x}) + V\left(\frac{\boldsymbol{x}}{\varepsilon}\right)\psi^\varepsilon(t,\boldsymbol{x}) \tag{3.16}$$

for one time step using the Bloch decomposition method, of which the intermediate steps shall be presented as follows.

Step 1.1. Take the Bloch transformation (2.12) of ψ^ε in (3.16), to obtain $\tilde{\psi}^\varepsilon$.

Step 1.2. Decompose $\tilde{\psi}^\varepsilon$ as a summation of the Bloch functions

$$\tilde{\psi}^\varepsilon(t,\boldsymbol{y},\boldsymbol{\xi}) = \sum_m c_m(t,\boldsymbol{\xi})\Psi_m(\boldsymbol{y},\boldsymbol{\xi}). \tag{3.17}$$

Step 1.3. Evolve the equation for $c_m(t,\boldsymbol{\xi})$ for one time step, where $c_m(t,\boldsymbol{\xi})$ satisfies

$$\mathrm{i}\varepsilon\partial_t c_m = E_m c_m, \tag{3.18}$$

and one gets

$$c_m(t+\Delta t,\boldsymbol{\xi}) = c_m(t,\boldsymbol{\xi})\exp\left(-\frac{\mathrm{i}}{\varepsilon}E_m(\boldsymbol{\xi})\Delta t\right). \tag{3.19}$$

Step 1.4. Obtain $\tilde{\psi}^\varepsilon$ at $t = t + \Delta t$ from

$$\tilde{\psi}^\varepsilon(t+\Delta t,\boldsymbol{y},\boldsymbol{\xi}) = \sum_m c_m(t+\Delta t,\boldsymbol{\xi})\Psi_m(\boldsymbol{y},\boldsymbol{\xi}). \tag{3.20}$$

Step 1.5 Apply the inverse Bloch transformation to $\tilde{\psi}^\varepsilon$ to get ψ^ε at $t + \Delta t$.

Step 2. Solve the ordinary differential equation

$$\mathrm{i}\varepsilon\partial_t\psi^\varepsilon = U(\boldsymbol{x})\psi^\varepsilon, \tag{3.21}$$

for one time step.

Clearly, the algorithm given above is frst order in time. But one can easily obtain a second order scheme by the Strang splitting method, *i.e.* perform Step 1 with time-step $\Delta t/2$, then Step 2 with Δt, and finally once again Step 1 with $\Delta t/2$.

As pointed out in [21, 22], for $\varepsilon \ll 1$, the BDTS method converges for the physical observables with a mesh size $O(\varepsilon)$ and time step $O(1)$, and thus has a huge advantage in improving the computational efficiency in comparison to the classical time splitting spectral method. However, such a mesh size is still too expensive in high dimension simulations and very small ε. In Section 4, we will propose a hybrid method which applies the BDTS method locally around the band-crossings to get the necessary quantum information, and for the rest part of domain, we apply the BDGB method to save the computational cost. For this purpose, we first implement the BDTS method locally around one point in the quasi-momentum space.

The local BDTS method. We give an 1D spatially discrete version of the Bloch decomposition method to show how to realize it and the extension to higher dimension is straightforward. Let the fundamental domain of the 1D lattice be $\mathcal{C} = [0,\, 2\pi]$ such that the first Brillouin zone of the reciprocal lattice is $\mathcal{B} = [-1/2,\, 1/2]$. Suppose we want to solve the periodic Schrödinger equation locally in quasi-momentum space B around the origin. Let a be a real number and $0 < a \le 1/2$, $L = 2a/\varepsilon \in \mathbb{N}$, and $R \in \mathbb{N}$, we discretize the local set $[-a,\, a] \in B$ and the fundamental domain $[0,\, 2\pi]$ as follows

$$\begin{cases} \xi_\ell = -a + (\ell-1)\varepsilon, & \text{for } \ell = 1, 2, ..., L, \\ y_r = \dfrac{2\pi(r-1)}{R}, & \text{for } r = 1, 2, ..., R, \end{cases} \tag{3.22}$$

and the mesh grid points in the spatial variable are

$$x_{\ell,r} = \varepsilon \left(\frac{\pi(\ell - 1)}{a} + y_r \right), \quad \text{for } \ell = 1, 2, ..., L \text{ and } r = 1, 2, ..., R. \tag{3.23}$$

Remark 3.2. The mesh grid given in (3.23) is the same as the original BDTS method given in [21, 22] when $a = 1/2$, in which one uses the BDTS method in the whole Brillouin zone, and a uniform mesh with $\Delta x = 2\pi/(LR)$. But when $a < 1/2$, the mesh is chosen differently – it is not uniform any more. We first divide the domain $[0, 2\pi]$ into L cells with size $\pi\varepsilon/a$, and then refine the mesh with mesh size $2\pi\varepsilon/R$ locally at each grid point $\pi\varepsilon(\ell - 1)/a$, see Figure 3.2 for an illustration.

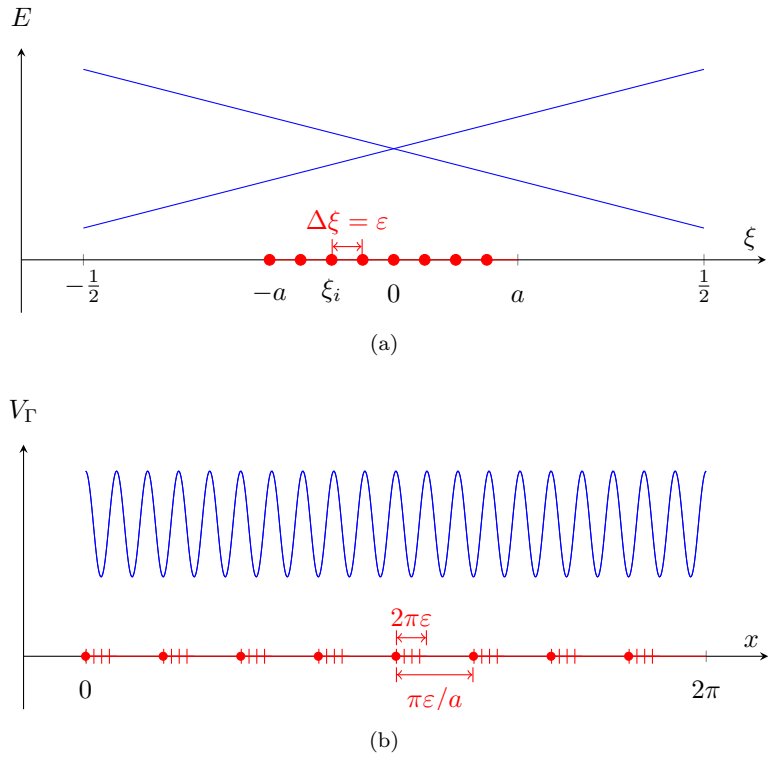

Figure 3.2: Illustration of the mesh points for the local BDTS method in 1D. (a) Mesh points in the momentum space. (b) Mesh points in the position space.

Suppose that at time t we are given $\psi^\varepsilon(t, x_{\ell,r}) = \psi_{\ell,r}$, then we do the following steps to obtain $\psi_{\ell,r}$ at time $t + \Delta t_{TS}$.

Step 1.1. Compute $\tilde{\psi}^{\varepsilon}(t, x_{\ell,r})$ by

$$\tilde{\psi}_{\ell,r} = \sum_{j=1}^{L} \psi_{j,r} \exp\left(-\mathrm{i}\,\xi_\ell\, x_{j,1}\right). \tag{3.24}$$

Step 1.2. Compute the m-th band Bloch coefficient $c_m(\xi)$ by

$$c_m(\xi_\ell) \approx c_{m,\ell} = \frac{2\pi}{R} \sum_{r=1}^{R} \tilde{\psi}_{\ell,r} \bar{\Psi}_m(y_r, \xi_\ell). \tag{3.25}$$

Step 1.3. Evolve $c_{m,\ell}$ up to time $t + \Delta t_{TS}$ by

$$c_{m,\ell} = c_{m,\ell} \exp\left(-\frac{\mathrm{i}}{\varepsilon} E_m(\xi_\ell) \Delta t_{TS}\right). \tag{3.26}$$

Step 1.4. Sum up all band contributions to obtain

$$\tilde{\psi}_{\ell,r} = \sum_{m} c_{m,\ell} \Psi_m(y_r, \xi_\ell). \tag{3.27}$$

Step 1.5 Take the inverse Bloch transformation to $\tilde{\psi}$ to find

$$\psi_{\ell,r} = \frac{1}{L} \sum_{j=1}^{L} \tilde{\psi}_{j,r} \exp\left(\mathrm{i}\,\xi_j\, x_{\ell,1}\right). \tag{3.28}$$

Step 2. Evolve the external potential part by

$$\psi_{\ell,r} = \psi_{\ell,r} \exp\left(-\frac{\mathrm{i}}{\varepsilon} U(x_{\ell,r}) \Delta t_{TS}\right). \tag{3.29}$$

Then one obtains $\psi_{\ell,r}$ as approximation of $\psi^{\varepsilon}(t + \Delta t_{TS}, x_{\ell,r})$ and one can repeat the above steps to get the final approximate solution.

4 A hybrid method

In this section we propose a hybrid method which combines the Bloch decomposition based Gaussian beam solver and time-splitting solver together. We want to gain the advantages from both of these two methods: the high efficiency of the BDGB method away from the band-crossing zone, and the high accuracy of the BDTS method around the band-crossings. A buffer zone is designed in order to exchange the data between the BDGB and BDTS solvers.

Without loss of generality, we assume that the only band-crossing point is the origin of the Brillouin zone. The basic idea of the hybrid method is shown in Figures 4.1 and 4.2 for

the 1D case and 2D case respectively. We solve the Schrödinger equation using the BDTS method in the domain $D_{TS} = [-a, a]^d$ where $d = 1, 2$ is the dimension, and outside the domain $[-c, c]^d$, *i.e.* , in $D_{GB} = B \setminus [-c, c]^d$, we use the BDGB method. The two domains D_{GB} and D_{TS} overlap in $D_{GB} \bigcap D_{TS}$, where waves going towards the outside direction of D_{TS} are converted to Gaussian beams, and Gaussian beams going inside of D_{TS} are converted to waves. The partition of different domains is similar to that in [23], but with a difference – in the case of this paper, the two buffer zones are not separated.

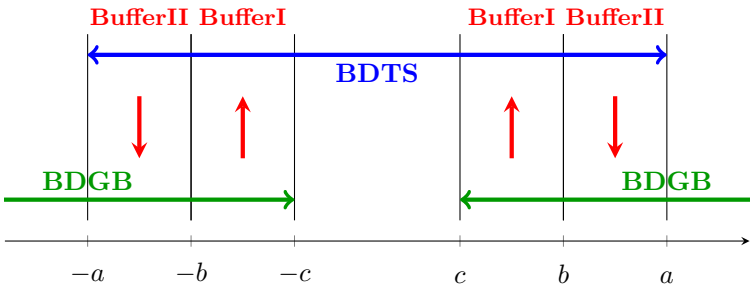

Figure 4.1: Illustration of the hybrid method in 1D

Away from the crossing point, the use of the asymptotic Gaussian beam solution can reduce the computational cost efficiently. Around the crossing point, the direct simulation of the Schrödinger equation by BDTS can capture the inter-band transitions, and one has to use fine spatial mesh and time steps of $O(\varepsilon)$ to get the desired accuracy, but since one can suitably choose the size of D_{TS} as $O(\sqrt{\varepsilon})$, the numerical cost of this part can also be reduced.

4.1 The main algorithm

We discretize the time by $t_n = n\Delta t$, and denote the time step using for the BDTS and BDGB as Δt_{TS} and Δt_{GB} respectively. Note that Δt is different from Δt_{TS} and Δt_{GB}. It is the time step between two steps of conversions in the buffer zones between Schrödinger waves and Gaussian beams. Generally, we choose $\Delta t \leq O(\sqrt{\varepsilon})$ and $\Delta t > \Delta t_{GB} > \Delta t_{TS}$. Then we proceed for the hybrid method in the following steps:

1. Initialization. From the initial data $\psi_0^\varepsilon(\boldsymbol{x})$ using the Bloch decomposition (2.18) and

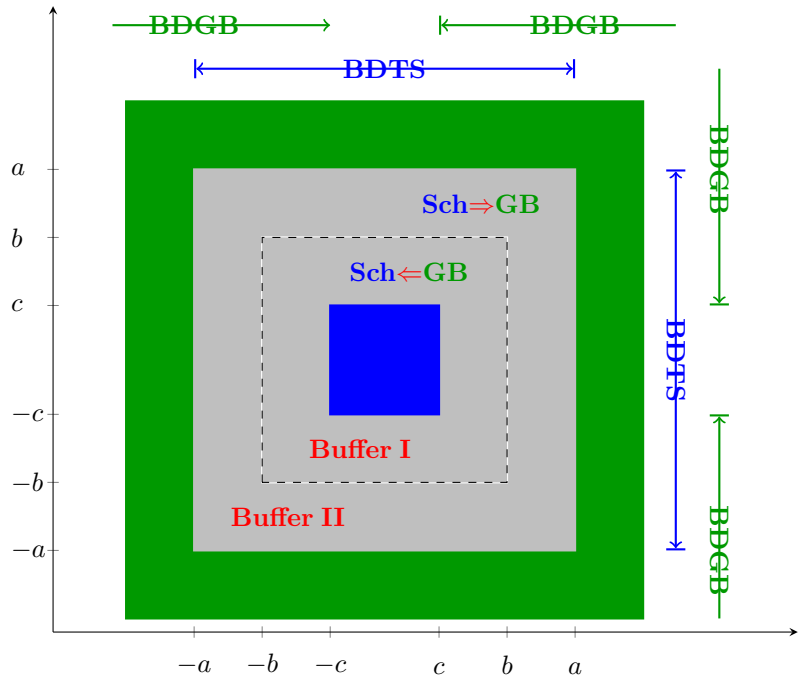

Figure 4.2: Illustration of the hybrid method in 2D

(2.19) to get the initial Bloch coefficient $c_m(t=0,\boldsymbol{\xi})$. Decompose $c_m(0,\boldsymbol{\xi})$ as

$$c_m(0,\boldsymbol{\xi}) = f_m(0,\boldsymbol{\xi}) + g_m(0,\boldsymbol{\xi}) + \mathrm{tol_m}, \quad m = 1, 2... \tag{4.1}$$

where g_m is defined as a series of Gaussian beams supported in D_{GB}, f_m has support in $B \setminus D_{GB}$, and $\mathrm{tol_m}$ is the numerical tolerance.

2. Main loops. In each time period $[t_n,\ t_{n+1}]$, do the following steps:

   2.1. Evolve $\{f_m(t,\boldsymbol{\xi})\}$ in D_{TS} using the BDTS method with time step Δt_{TS} to obtain $\{f_m^*(\boldsymbol{\xi})\}$;

   2.2. Evolve $\{g_m(t,\boldsymbol{\xi})\}$ in D_{GB} using the BDGB method with time step Δt_{GB} to obtain $\{g_m^*(\boldsymbol{\xi})\}$;

   2.3. Call subroutine Sch2GB with input $(f_m^*,\ g_m^*)$ to convert the BDTS data to BDGB data in Buffer II and get $(f_m^{**},\ g_m^{**})$.

   2.4. Call subroutine GB2Sch with input $(f_m^{**},\ g_m^{**})$ to convert the BDGB data to BDTS data in Buffer I and get $(f_m(t_{n+1}),\ g_m(t_{n+1}))$.

3. Reconstruction. At the final time $t = t_N$, we compute

$$c_m(t, \boldsymbol{\xi}) = f_m(t, \boldsymbol{\xi}) + g_m(t, \boldsymbol{\xi}), \quad m = 1, 2... \tag{4.2}$$

and reconstruct the Schrödinger solution $\psi^\varepsilon(t, \boldsymbol{x})$ using (2.18) and (2.15).

Basically the two subroutine Sch2GB and GB2Sch decompose f_m into Gaussian beams in the buffer zone, and check their directions of motion. If a Gaussian beam is in Buffer II and it is going outwards from the origin, we subtract it from f_m and add it to g_m; if a Gaussian beam is in Buffer I and it is going towards the origin, we subtract it from g_m and add it to f_m.

4.1.1 The data exchange routines

The algorithm Sch2GB. Input: (f, g); Output (f, g). This subroutine is used to extract Gaussian beams from the wavefunction in the buffer zone. We use tol_1 and tol_2 to denote two (small) numerical tolerances.

1. Determine whether to start the conversion. Define a smooth damping function $L_{a,b}(\boldsymbol{\xi})$ with support in $\left\{\boldsymbol{\xi} \in \mathbb{R}^d \,|\, \|\boldsymbol{\xi}\|_\infty \in [b,\, a]\right\}$. Define $P = \int |f(\boldsymbol{\xi}) L_{a,b}(\boldsymbol{\xi})| \,\mathrm{d}\xi$ and check if $(P < \mathrm{tol}_1)$. If so, which means the wavefunction f is small enough, then end this algorithm and return;
2. Define $f_L(\boldsymbol{\xi}) = f(\boldsymbol{\xi}) L_{a,c}(\boldsymbol{\xi})$ and $k =$ number of Gaussian beams in g, *i.e.* $g(\boldsymbol{\xi}) = \sum_{i=1}^k g_i(\boldsymbol{\xi})$, where each g_i is a Gaussian beam function;
3. Extract outgoing Gaussian beams from the wavefunction f in the buffer zone. Let $g_{tmp} = 0$;

   while $(P > \mathrm{tol}_2)$ **do**

   Extract a Gaussian beam $\tilde{g}(\boldsymbol{\xi})$ from $f_L(\boldsymbol{\xi})$, where

   $$\tilde{g}(\boldsymbol{\xi}) = a \exp\left(-\frac{\mathrm{i}}{\varepsilon}\left(\boldsymbol{x} \cdot (\boldsymbol{\xi} - \boldsymbol{p}) + \frac{1}{2} M (\boldsymbol{\xi} - \boldsymbol{p})^2\right)\right);$$

   $f_L = f_L - \tilde{g}; \quad P = \int |f_L(\boldsymbol{\xi}) L_{a,b}(\boldsymbol{\xi})| \,\mathrm{d}\xi;$

   if $((\boldsymbol{p} \in$ Buffer II$)$ & $(\boldsymbol{p} \cdot (-\nabla_{\boldsymbol{x}} U(\boldsymbol{x})) < 0))$ **then**

   !# $\tilde{g}$ is going towards the origin. Do not convert.

   Break the do loops;

   end if

   $k = k + 1; \quad g_k = \tilde{g}; \quad g_{tmp} = g_{tmp} + \tilde{g};$

end while

4. Subtract the outgoing Gaussian beams from the wavefunction f, *i.e.* $f = f - g_{tmp}$.

The algorithm GB2Sch. Input: (f, g); Output (f, g). This subroutine is used to convert the Gaussian beams to the wavefunction, and is applied to each beam in the buffer zone.

1. Find the Gaussian beams to be converted. For each of the Gaussian beams, g_k in g, check its parameters $\boldsymbol{p}_k$ and $\boldsymbol{x}_k$. Select the Gaussian beams whose $\boldsymbol{p}_k$ are in Buffer I and $(\boldsymbol{p} \cdot (-\nabla_{\boldsymbol{x}} U(\boldsymbol{x})) < 0)$ (going towards the origin);
2. Check the support of the selected Gaussian beams in the first step. If the support of g_k is contained in $[-b, b]^d$, add g_k to f and subtract it from g; If not, we need to decompose g_k into smaller beams and only add and subtract those whose supports are in $[-b, b]^d$.

The method we used in the algorithm Sch2GB to extract Gaussian beams from a oscillatory function comes from [23, 38]. It looks for the Gaussian beam parameter that minimize the difference between the given oscillatory function and the Gaussian beam.

4.2 The numerical example for the hybrid method

4.2.1 The numerical example in 1D

In this subsection we give an example of the hybrid method in one dimensional space. We solve the Schrödinger equation (2.7) with the periodic potential $V_\Gamma(x) = \cos(x)$. The initial data is chosen as a wave packet projected on to the 4-th Bloch band with the following form

$$\begin{aligned} \psi_0^\varepsilon(x) &= \mathbb{P}_4 \left(a_0(x) \mathrm{e}^{\frac{\mathrm{i}}{\varepsilon}\xi_0 x} \right), \quad \text{with } \xi_0 = -1/4, \\ a_0(x) &= \left(\frac{8}{\varepsilon\pi} \right)^{\frac{1}{4}} \exp\left(-\frac{4(x-\pi)^2}{\varepsilon} \right). \end{aligned} \tag{4.3}$$

The external potential is chosen as a linear potential $U(x) = -x$.

Remark 4.1. In this example, we project the initial data onto the 4-th Bloch band of the Mathieu's model (see Figure 2.3 for the band structure). By choosing the external potential as $U(x) = -x$, semi-classically the wave packet is dragged to the right in the quasi-momentum space. And furthermore one can think about the wave evolving in a

subsystem with only the 4-th and 5-th Bloch bands included since others are well separated from these two. We then call the 4-th band and 5-th band as the lower band and the upper band respectively.

The Buffer zones shown in Figure 4.1 are set by $(a, b, c) = (8\sqrt{\varepsilon}, 4\sqrt{\varepsilon}, \sqrt{\varepsilon})$.

We compare the result computed from the hybrid method with the "exact" solution which is computed using the BDTS method with the mesh size and time step small enough.

In Table 4.1, we show the L^2-errors between the Schrödinger solution ψ^ε and the solution ψ^ε_{hyb} by the hybrid method. In Figure 4.3 we plot the densities and the absolute errors for different ε. In Figure 4.4 we plot the population at the lower Bloch band as a function of time and one can see that transitions happen around time $t = 0.25$ when the wave packet hits the crossing point.

Table 4.1: Numerical example in 4.2.1: The L^2-errors of wave function for the hybrid method at $t = 1/2$.

ε	2^{-9}	2^{-10}	2^{-11}	2^{-12}	2^{-13}
$\|\psi^\varepsilon - \psi^\varepsilon_{GB}\|_2$	4.06E-2	1.37E-2	1.20E-2	2.84E-3	1.56E-3

4.2.2 A numerical example in 2D

We give an example for the 2D Schrödinger equation (2.7) with a honeycomb lattice potential given in (2.6). Set $\varepsilon = 2^{-10}$ and the initial data is chosen as

$$\psi^\varepsilon_0(\boldsymbol{x}) = \mathbb{P}_1 \left(a_0(\boldsymbol{x}) \mathrm{e}^{\frac{\mathrm{i}}{\varepsilon}\boldsymbol{\xi}_0 \cdot \boldsymbol{x}} \right), \tag{4.4}$$

$$a_0(\boldsymbol{x}) = \exp\left(-32(\boldsymbol{x} - \pi)^2\right), \tag{4.5}$$

where $\boldsymbol{\xi}_0 = (1/2, 1/2)$. This will generate a wave packet located at $\boldsymbol{\xi}_0$ in the quasi-momentum space. The external potential is given by

$$U(x_1, x_2) = -x_1 + x_2, \tag{4.6}$$

so that $-\nabla_{\boldsymbol{x}} U = (1, -1)$, and semi-classically the trajectory of $\boldsymbol{\xi}$ will move directly into the Dirac point $\boldsymbol{\xi}^* = (2/3, 1/3)$. The domains are defined by $[a,\, b,\, c] = [4\sqrt{\varepsilon},\, 2.5\sqrt{\varepsilon},\, \sqrt{\varepsilon}]$. For the BDTS method, we use $\Delta x = \varepsilon/16$ and $\Delta t_{TS} = \varepsilon/2$; and for the BDGB method, we use a 4-th order Runge-Kutta method with $\Delta t_{GB} = \sqrt{\varepsilon}/8$.

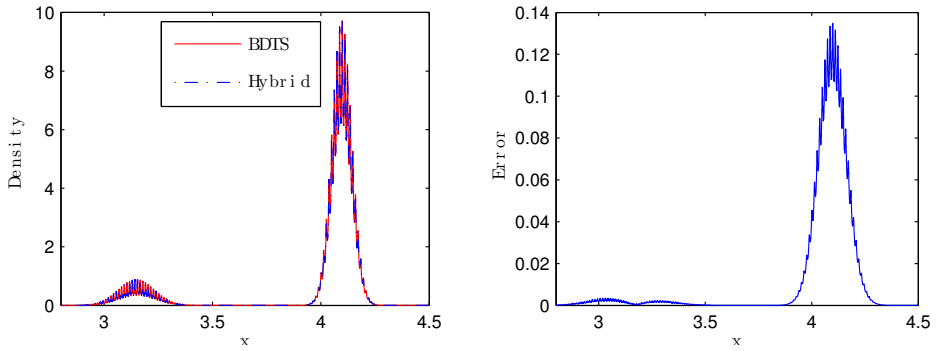

(a) $\varepsilon = 2^{-9}$

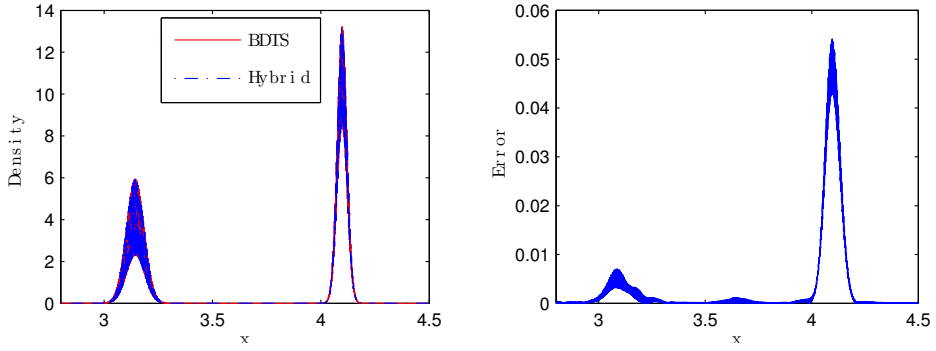

(b) $\varepsilon = 2^{-11}$

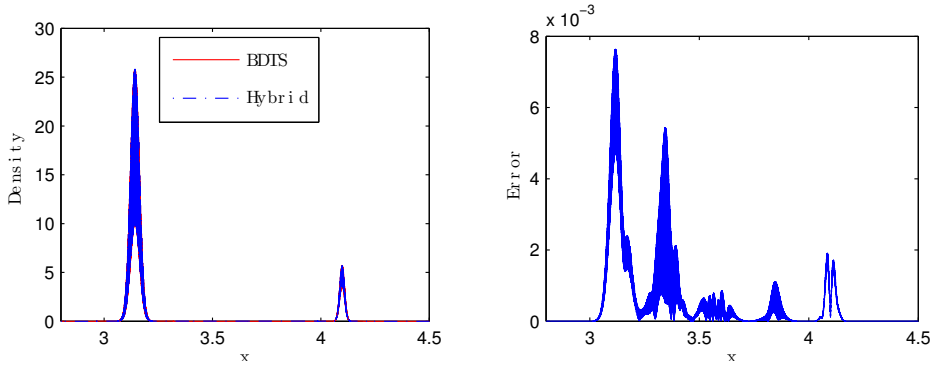

(c) $\varepsilon = 2^{-13}$

Figure 4.3: Numerical example in 4.2.1: The Schrödinger solution versus the hybrid solution. Left column: the comparisons of the density at time $t = 1/2$; right column: the absolute error between the Schrödinger solution and the hybrid solution.

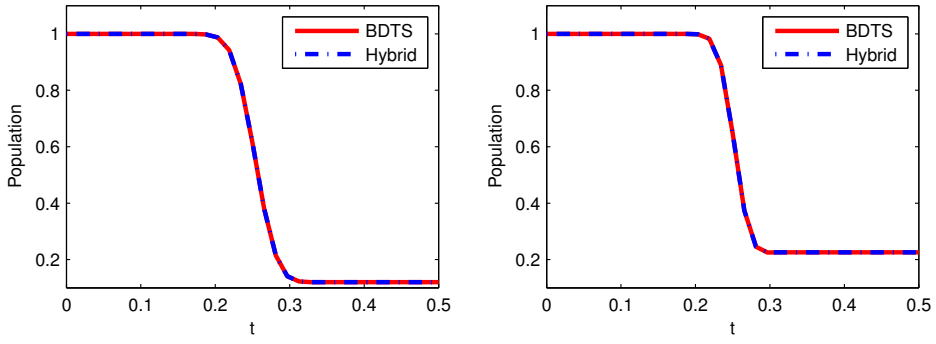

(a) $\varepsilon = 2^{-9}$ (b) $\varepsilon = 2^{-10}$

(c) $\varepsilon = 2^{-11}$ (d) $\varepsilon = 2^{-12}$

Figure 4.4: Numerical example in 4.2.1: Particle population in the lower Bloch band as function of time.

Figure 4.5 shows the results computed by the hybrid method at different times. We can see the hybrid method captures a clear inter-band transition happening at the Dirac point $\boldsymbol{\xi}^* = (2/3, 1/3)$.

We remark here that the Schrödinger equation with a honeycomb lattice potential can be used to model the electron motion in a Graphene layer, and due to the existence of the Dirac point, inter-band transitions are very important in the simulations. But since this problem is defined in two dimensional space, when ε is small, to solve (1.1) using the BDTS method will be a huge challenge for the memory and cpu time. With the help of the hybrid method, this example can be done in one hour on a personal laptop.

4.2.3 The Klein paradox in the Schrödinger equation

We use the Schrödinger equation with a honeycomb lattice potential to model the motion of electron in a graphene sheet structure. One of the important phenomena in graphene is Klein tunneling (*e.g.* [27, 37, 41]), which is a form of potential scattering originally associated with the Dirac equation. The Klein paradox happens when a particle approaches a sharp rectangular potential barrier. In nonrelativistic quantum mechanics, electron tunneling into a barrier is observed with exponential damping. But for the relativistic particle the barrier can be nearly transparent, which is the so called Klein tunneling [28]. For the Graphene layer, due to the band structure and the existence of the Dirac points (as shown in Figure 2.4), one can expect to see the Klein tunneling [27], first observed in graphene experimentally in [37, 41]. Most of the studies on the Klein tunneling were considering step potentials or square barriers which are highly idealized. In [36] the Klein tunneling was investigated using a smooth potential which is given by hyperbolic tangent functions. In this subsection, we explore this idea to approximate a step potential by a hyperbolic tangent function and give a numerical example applying the hybrid method.

We consider the Schrödinger equation (2.7) with the honeycomb lattice potential given in (2.6), and the external potential given by

$$U(\boldsymbol{x}) = U(x_1, x_2) = \frac{1}{2} U_0 \left(\tanh\left(\frac{x_1 - \pi}{w} \right) + 1 \right), \tag{4.7}$$

where U_0 is a constant that corresponds to the height of the step potential and w is a constant corresponding the transition distance of the step potential. Notice that when $w \to 0$, $U(\boldsymbol{x})$ approximates a step potential that attains the value 0 for $x_1 \leq 0$ and U_0 for $x_1 > 0$. The

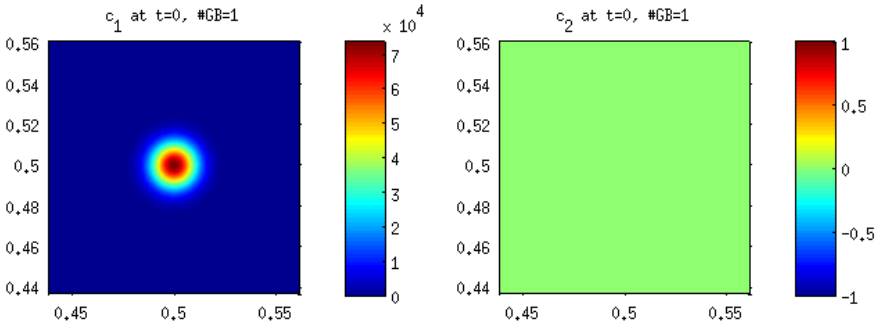

(a)

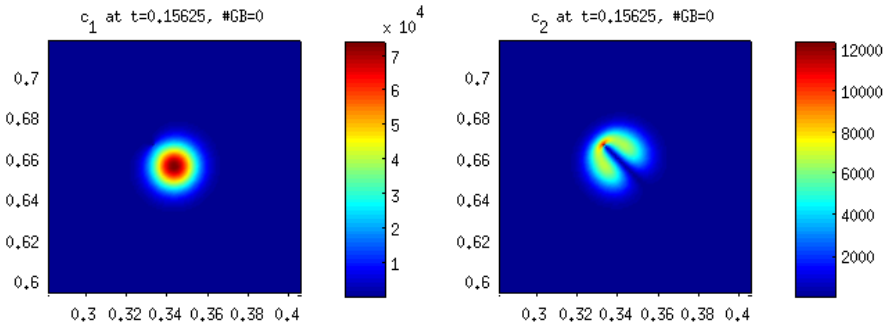

(b)

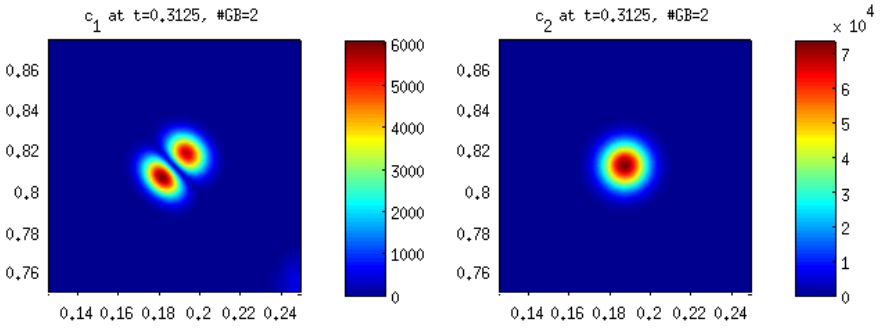

(c)

Figure 4.5: Numerical example in 4.2.2: Solutions at different time by the hybrid method. Left column: $|c_1(t,\boldsymbol{\xi})|$, right column: $|c_2(t,\boldsymbol{\xi})|$. $\sharp GB$ is the number of Gaussian beams used for the simulation.

initial value is given by

$$\psi_0^\varepsilon(\boldsymbol{x}) = \mathbb{P}_2 \left(\exp\left(-32(\boldsymbol{x}-\boldsymbol{x}_0)^2\right) \mathrm{e}^{\frac{\mathrm{i}}{\varepsilon}\boldsymbol{\xi}_0\cdot\boldsymbol{x}} \right). \tag{4.8}$$

In this numerical example, we set $\varepsilon = 2^{-10}$, $V_0 = -0.6266$, $U_0 = 0.0315$, $w = 0.05$, $\boldsymbol{x}_0 = (\pi - 1, 1.5\pi)$ and $\boldsymbol{\xi}_0 = (0.7450, 0.3333)$. With these choices of the constants, initially the wavepacket is located at $\boldsymbol{\xi}_0$ in the second Bloch band with energy $E_2(\boldsymbol{\xi}_0) = 0.0232$ which is smaller than the step height U_0. We then apply the hybrid method in solving this problem numerically. As time evolves, the wavepacket moves towards to the step potential and we show the numerical position density in Figure 4.6. Notice that in Figure 4.6 we plot the results in the real spatial $\boldsymbol{r}$-coordinate instead of the computational $\boldsymbol{x}$-coordinate, where $\boldsymbol{r}$ and $\boldsymbol{x}$ are related by the lattice transformation $\boldsymbol{r} = Q\boldsymbol{x}$ in (2.1). We can see initially (top plot) the wave packet away from the step (whose location is indicated by the light straight line across the diagonal), and it "hits" the potential step at $t = 3$ (middle plot). One can see the major part of the wavepacket "tunnels" through the potential step while only a slight part is reflected (bottom plot).

5 The Dirac approximation

5.1 The Dirac equation as the limit of the Schrödinger equation

At the Dirac point, it has been shown that the Schrödinger equation (1.1) has a limit governed by the 2D Dirac equation [16, 17, 3].

We consider the Schrödinger equation (1.1) in the case of V_Γ being a periodic potential w.r.t the honeycomb lattice Γ. The Bloch functions Ψ_m, $m = 1, 2, ...$, are obtained by solving the eigenvalue problem

$$\begin{aligned} \left(-\frac{1}{2}\Delta_{\boldsymbol{r}} + V_\Gamma(\boldsymbol{r})\right) \Psi_m(\boldsymbol{r},\boldsymbol{p}) &= E_m(\boldsymbol{p})\, \Psi_m(\boldsymbol{r},\boldsymbol{p}), \\ \Psi(\boldsymbol{r}+\boldsymbol{v},\boldsymbol{p}) &= \mathrm{e}^{\mathrm{i}\boldsymbol{p}\cdot\boldsymbol{v}}\, \Psi(\boldsymbol{r},\boldsymbol{p}), \quad \forall \boldsymbol{v} \in \Gamma. \end{aligned} \tag{5.1}$$

In [16], it has been shown that the first two Bloch bands denoted by $E_1(\boldsymbol{p})$ and $E_2(\boldsymbol{p})$, with corresponding eigenfunctions $\Psi_1(\boldsymbol{r},\boldsymbol{p})$ and $\Psi_2(\boldsymbol{r},\boldsymbol{p})$ respectively, have conical crossings at the Dirac points. Assuming $\boldsymbol{K}^*$ is a Dirac point of $\boldsymbol{K}$ or $\boldsymbol{K}'$ type for the honeycomb lattice potential V_Γ, and at $\boldsymbol{p} = \boldsymbol{K}^*$, $E_1(\boldsymbol{K}^*) = E_2(\boldsymbol{K}^*) = \mu$. Furthermore, at $\boldsymbol{K}^*$ the eigenfunctions can be chosen with certain symmetry. More precisely one can have the following properties (Proposition 2.2 and Theorem 4.1 in [16]):

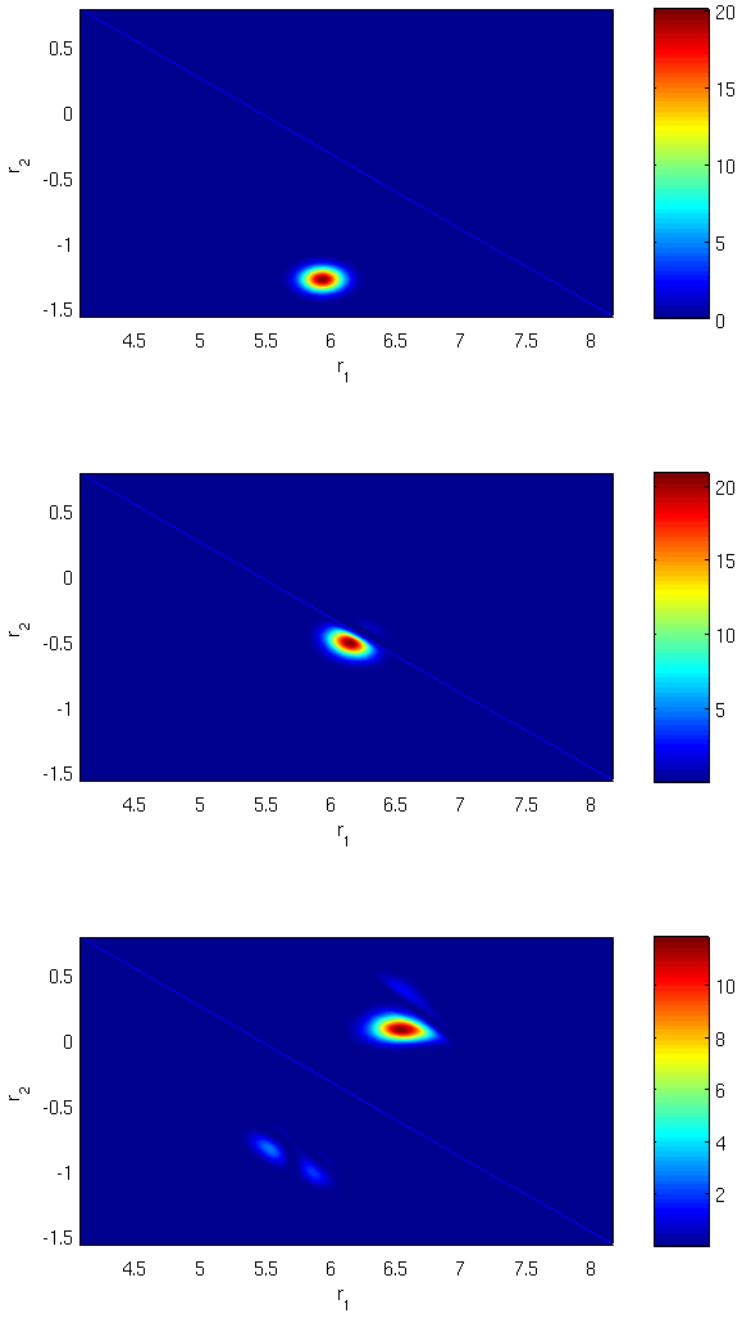

Figure 4.6: Numerical example in 4.2.3: Position density $|\psi^\varepsilon|^2$ at different time by the hybrid method. Top: $t = 0$; middle: $t = 3$; bottom: $t = 6$.

Proposition 5.1. *If $\Psi(\boldsymbol{r},\boldsymbol{p})$ is an eigenfunction with $\boldsymbol{p}=\boldsymbol{K}^*$, then $\mathcal{R}[\Psi(\cdot,\boldsymbol{p})](\boldsymbol{r})$ is also an eigenfunction with $\boldsymbol{p}=\boldsymbol{K}^*$. Here the rotation operator $\mathcal{R}$ is defined by*

$$\mathcal{R}[f](\boldsymbol{r}) = f(R^T\boldsymbol{r}), \quad \text{for any function } f, \tag{5.2}$$

in which the matrix R is the $2\pi/3$-clockwise-rotation matrix:

$$R = \begin{pmatrix} -\frac{1}{2} & \frac{\sqrt{3}}{2} \\ -\frac{\sqrt{3}}{2} & -\frac{1}{2} \end{pmatrix}. \tag{5.3}$$

Proposition 5.2. *At the Dirac point $\boldsymbol{K}^*$, there exists an eigenfunction $\Psi_1(\boldsymbol{r}) = \Psi_1(\boldsymbol{r},\boldsymbol{K}^*)$ corresponding to the eigenvalue μ such that the following statements hold:*

1. *$\mathcal{R}[\Psi_1](\boldsymbol{r}) = \tau\Psi_1(\boldsymbol{r})$ with $\tau = \mathrm{e}^{2\pi\mathrm{i}/3}$;*
2. *$\Psi_2(\boldsymbol{r}) := \overline{\Psi_1(-\boldsymbol{r})}$ is also an eigenfunction corresponding to the eigenvalue μ;*
3. *$\mathcal{R}[\Psi_2](\boldsymbol{r}) = \bar{\tau}\Psi_2(\boldsymbol{r})$;*
4. *$\langle\Psi_m,\Psi_n\rangle = \delta_{mn}$, $m,n=1,2$;*
5. *$\{\Psi_1,\Psi_2\}$ spans the eigenspace corresponding the eigenvalue μ.*

We call Ψ_1 and Ψ_2 the Dirac-eigenfunctions.

From now on, in this section we will denote $\Psi_1 = \Psi_1(\boldsymbol{r},\boldsymbol{K}^*)$ and $\Psi_2 = \Psi_2(\boldsymbol{r},\boldsymbol{K}^*)$ as the two Dirac-eigenfunctions satisfying the properties in Proposition 5.2. Assume that the initial data of (1.1) are given by

$$\psi^\varepsilon(t=0,\boldsymbol{r}) = \alpha_1^0(\boldsymbol{r})\Psi_1\left(\frac{\boldsymbol{r}}{\varepsilon}\right) + \alpha_2^0(\boldsymbol{r})\Psi_2\left(\frac{\boldsymbol{r}}{\varepsilon}\right). \tag{5.4}$$

We look for the solution with the ansatz

$$\psi^\varepsilon(t,\boldsymbol{r}) = \mathrm{e}^{-\mathrm{i}\mu t/\varepsilon}\left(\alpha_1(t,\boldsymbol{r})\Psi_1\left(\frac{\boldsymbol{r}}{\varepsilon}\right) + \alpha_2(t,\boldsymbol{r})\Psi_2\left(\frac{\boldsymbol{r}}{\varepsilon}\right)\right). \tag{5.5}$$

Define the fast variable $\boldsymbol{z} = \boldsymbol{r}/\varepsilon$, then $\nabla_{\boldsymbol{r}} \to \nabla_{\boldsymbol{r}} + \frac{1}{\varepsilon}\nabla_{\boldsymbol{z}}$. Plugging (5.5) into (1.1), one gets

$$\begin{aligned} \mathrm{i}\varepsilon\sum_{m=1}^{2}\partial_t\alpha_m(t,\boldsymbol{r})\Psi_m(\boldsymbol{z}) = &-\varepsilon\sum_{m=1}^{2}\nabla_{\boldsymbol{r}}\alpha_m(\boldsymbol{r})\cdot\nabla_{\boldsymbol{z}}\Psi_m(\boldsymbol{z}) + U\sum_{m=1}^{2}\alpha_m\Psi_m(\boldsymbol{z}) \\ &-\frac{\varepsilon^2}{2}\sum_{m=1}^{2}\Delta_{\boldsymbol{r}}\alpha_m\Psi_m(\boldsymbol{z}). \end{aligned} \tag{5.6}$$

Formally if one assumes $U = O(\varepsilon)$, neglects the $O(\varepsilon^2)$ term in (5.6), and takes inner product w.r.t Ψ_1 and Ψ_2, one gets

$$\partial_t \alpha_n = \mathrm{i} \sum_{m=1}^{2} \langle \nabla_{\boldsymbol{z}} \Psi_m, \Psi_n \rangle \cdot \nabla_{\boldsymbol{r}} \alpha_m - \frac{\mathrm{i}}{\varepsilon} U \alpha_m, \quad m = 1, 2. \tag{5.7}$$

From Theorem 4.1 and Proposition 4.2 of [16], one has

$$\mathrm{i}\langle \nabla_{\boldsymbol{z}} \Psi_1, \Psi_1 \rangle = \mathrm{i}\langle \nabla_{\boldsymbol{z}} \Psi_2, \Psi_2 \rangle = 0, \tag{5.8}$$

$$\mathrm{i}\langle \nabla_{\boldsymbol{z}} \Psi_2, \Psi_1 \rangle = \overline{\mathrm{i}\langle \nabla_{\boldsymbol{z}} \Psi_1, \Psi_2 \rangle} = -\bar{\lambda}_\sharp \begin{pmatrix} 1 \\ \mathrm{i} \end{pmatrix}, \tag{5.9}$$

where $\lambda_\sharp$ is a complex-valued constant. Then from (5.7) one gets the following Dirac equations:

$$\begin{aligned} \partial_t \alpha_1 &= -\bar{\lambda}_\sharp \left(\partial_{r_1} \alpha_2 + \mathrm{i} \partial_{r_2} \alpha_2 \right) - \frac{\mathrm{i}}{\varepsilon} U \alpha_1, \\ \partial_t \alpha_2 &= -\lambda_\sharp \left(\partial_{r_1} \alpha_1 - \mathrm{i} \partial_{r_2} \alpha_1 \right) - \frac{\mathrm{i}}{\varepsilon} U \alpha_2. \end{aligned} \tag{5.10}$$

So now formally one has the Dirac equations (5.10) as a limit of the Schrödinger equation (1.1). We refer to [17] for the rigorous proof of this limit when U is zero or small, however in the case of $U = O(1)$ the limit is not clear and formally it violates the asymptotics in getting (5.7).

5.2 Numerical verification of the Dirac limit

In this subsection, we numerically test the Dirac approximation to the Schrödinger equation when ε is small in different cases. For the convenience of computation, we use the $\boldsymbol{x}$-variable representation, that is $\boldsymbol{x} = (x_1, x_2)^T = A^T \boldsymbol{r}$, and (5.10) is equivalent to the following Dirac type system

$$\begin{aligned} \partial_t \alpha_1(t, \boldsymbol{x}) &= -\bar{\lambda}_\sharp (1, \mathrm{i}) \cdot \nabla_{\boldsymbol{x}}^A \alpha_2(t, \boldsymbol{x}) - \frac{\mathrm{i}}{\varepsilon} U(\boldsymbol{x}) \alpha_1(t, \boldsymbol{x}), \\ \partial_t \alpha_2(t, \boldsymbol{x}) &= -\lambda_\sharp (1, -\mathrm{i}) \cdot \nabla_{\boldsymbol{x}}^A \alpha_1(t, \boldsymbol{x}) - \frac{\mathrm{i}}{\varepsilon} U(\boldsymbol{x}) \alpha_2(t, \boldsymbol{x}). \end{aligned} \tag{5.11}$$

Then from the solution of (5.11) one can construct

$$\psi_{\mathrm{Dirac}}^\varepsilon(t, \boldsymbol{x}) = \mathrm{e}^{-\mathrm{i}\mu t/\varepsilon} \left(\alpha_1(t, \boldsymbol{x}) \Psi_1 \left(\frac{\boldsymbol{x}}{\varepsilon} \right) + \alpha_2(t, \boldsymbol{x}) \Psi_2 \left(\frac{\boldsymbol{x}}{\varepsilon} \right) \right), \tag{5.12}$$

as an asymptotic solution of

$$\mathrm{i}\varepsilon \partial_t \psi^\varepsilon(t, \boldsymbol{x}) = -\frac{\varepsilon^2}{2} \left(\nabla^A \right)^2 \psi^\varepsilon(t, \boldsymbol{x}) + \left(V_\Gamma \left(\frac{\boldsymbol{x}}{\varepsilon} \right) + U(\boldsymbol{x}) \right) \psi^\varepsilon(t, \boldsymbol{x}). \tag{5.13}$$

To verify the Dirac limit numerically, we choose the periodic potential as (2.6) and the Dirac point at $\boldsymbol{K}^* = \frac{1}{3}(\boldsymbol{k}_2 - \boldsymbol{k}_1)$. The first two Bloch bands have a cross at $\boldsymbol{K}^*$ with same eigenvalue $E_1(\boldsymbol{K}^*) = E_2(\boldsymbol{K}^*) = -0.6266$, and the Dirac-eigenfunctions can be chosen as shown in Figure 5.1. The constant $\lambda_\sharp$ in the Dirac equations given by these two Dirac-eigenfunctions is $\lambda_\sharp = 0.2081 + 0.1418\,\mathrm{i}$.

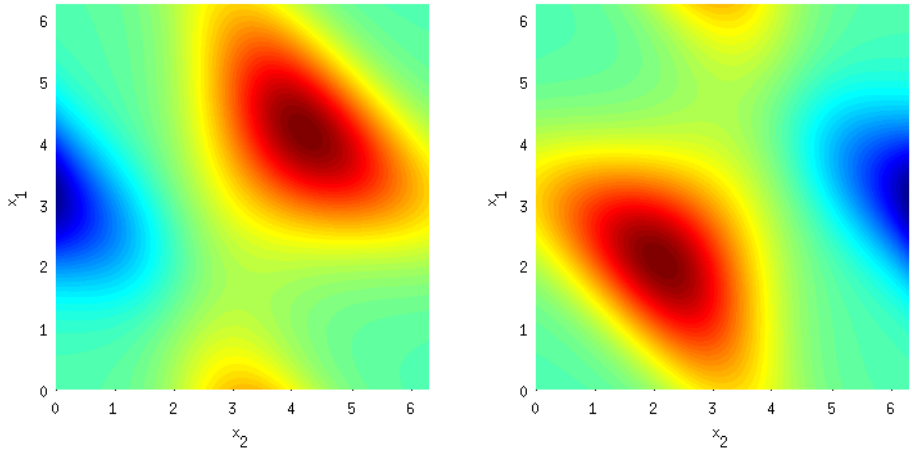

(a) Real part of Ψ_1 (b) Real part of Ψ_2

Figure 5.1: The Dirac-eigenfunctions.

We choose the initial data for (5.11) as (5.4) with

$$\alpha_1^0 = \exp\big(-2(\boldsymbol{x} - \pi)^2\big), \quad \alpha_2^0 = 0, \tag{5.14}$$

and then compare the solutions from both the Schrödinger equation (5.13) and the Dirac equations (5.11)-(5.12) for the following choices of the potential U:

$$U_1 \equiv 0; \quad U_2 = \varepsilon(\boldsymbol{x} - \pi)^2; \quad U_3 = (\boldsymbol{x} - \pi)^2. \tag{5.15}$$

The Schrödinger equation (5.13) is computed by the Bloch decomposition based time splitting method [21] and the Dirac equation (5.11) is computed by the Fourier spectrum time splitting method [5]. We compute the L^2 error between the two solutions

$$\mathrm{Err}^\varepsilon = \left(\int |\psi^\varepsilon(t, \boldsymbol{x}) - \psi^\varepsilon_{\mathrm{Dirac}}(t, \boldsymbol{x})|^2 \mathrm{d}\boldsymbol{x} \right)^{1/2}. \tag{5.16}$$

The errors for different potential U and ε are shown in Table 5.1, where we have used $\mathrm{Err}_i^\varepsilon$ to denote the L^2 error when $U = U_i$. We can see that when the external potential is

small ($U \equiv 0$ and $U = \varepsilon(\boldsymbol{x} - \pi)^2$) the errors are of $O(\varepsilon)$, which indicates that the Dirac equation is a good approximation to the Schrödinger equation in the semiclassical regime. However, when choosing $U = (\boldsymbol{x} - \pi)^2$, the errors are $O(1)$, which means that the Dirac solution does not converge to the Schrödinger solution as ε deceases. As we have seen from (5.10), the $O(1)$ external potential U will break down the formal asymptotics and forcing the momentum away from the Dirac point, which cause the $O(1)$ errors.

Table 5.1: The errors between the Dirac and the Schrödinger solutions at time $t = 0.5$. $\mathrm{Err}_i^\varepsilon$ is computed by choosing $U = U_i$, $i = 1, 2, 3$.

Time step ε	2^{-4}	2^{-5}	2^{-6}	2^{-7}
$\mathrm{Err}_1^\varepsilon$	1.25E-01	6.19E-02	3.08E-02	1.54E-02
$\mathrm{Err}_2^\varepsilon$	1.28E-01	6.33E-02	3.16E-02	1.58E-02
$\mathrm{Err}_3^\varepsilon$	5.31E-01	6.64E-01	8.47E-01	1.04E00

6 Conclusion

In order to deal with inter-band transitions in the case of band-crossing, we have built up a Bloch decomposition-based hybrid method. The Bloch decomposition-based Gaussian beam method is used away from the crossing point and the Bloch decomposition-based time splitting method is used locally around the crossing point. We have seen that this method has a great advantage in saving computational cost while it can capture the inter-band transition phenomena properly. Moreover, this method can be used in simulating electronic behavior in a graphene layer as shown in the numerical examples. In addition, we show that the Schrödinger equation converges to the Dirac equations when the external potential is zero or small, but does not converge for general external potentials.

References

[1] M. J. Ablowitz, C. W. Curtis, and Y. Zhu. On tight-binding approximations in optical lattices. *Studies in Applied Mathematics*, 129(4):362–388, 2012.

[2] M. J. Ablowitz and Y. Zhu. Nonlinear waves in shallow honeycomb lattices. *SIAM Journal on Applied Mathematics*, 72(1):240–260, 2012.

[3] J. Arbunich and C. Sparber. Rigorous derivation of nonlinear Dirac equations for wave propagation in honeycomb structures.

[4] N. Ashcroft and N. Mermin. *Solid State Physics*. Science: Physics. Saunders College, 1976.

[5] W. Bao, S. Jin, and P. Markowich. On time-splitting spectral approximations for the Schrödinger equation in the semiclassical regime. *Journal of Computational Physics*, 175(2):487–524, 2002.

[6] P. Bechouche. Semi-classical limits in a crystal with a coulombian self-consistent potential: Effective mass theorems. *Asymptotic Analysis*, 19(2):95–116, 1999.

[7] P. Bechouche, N. J. Mauser, and F. Poupaud. Semiclassical limit for the schrödinger-poisson equation in a crystal. *Communications on Pure and Applied Mathematics*, 54(7):851–890, 2001.

[8] A. Bensoussan, J.-L. Lions, and G. Papanicolaou. *Asymptotic analysis for periodic structures*, volume 374. American Mathematical Soc., 2011.

[9] F. Bloch. Über die quantenmechanik der elektronen in kristallgittern. *Zeitschrift für Physik A Hadrons and Nuclei*, 52(7):555–600, 1929.

[10] A. Bohm, A. Mostafazadeh, H. Koizumi, Q. Niu, and J. Zwanziger. *The Geometric Phase in Quantum Systems: Foundations, Mathematical Concepts, and Applications in Molecular and Condensed Matter Physics*. Theoretical and Mathematical Physics. Springer, 2010.

[11] G. Borgioli, O. Morandi, G. Frosali, and M. Modugno. Different approaches for multi-band transport in semiconductors. *Ukrainian Mathematical Journal*, 57(6):883–890, 2005.

[12] R. Carles, P. Markowich, and C. Sparber. Semiclassical asymptotics for weakly nonlinear Bloch waves. *Journal of Statistical Physics*, 117(1):343–375, 2004.

[13] L. Chai, S. Jin, and Q. Li. Semi-classical models for the Schrödinger equation with periodic potentials and band crossings. *Kinetic and Related Models*, 6(3):505–532, 2013.

[14] R. Delgadillo, J. Lu, and X. Yang. Gauge-invariant frozen gaussian approximation method for the schrodinger equation with periodic potentials. *SIAM Journal on Scientific Computing*, 38(4):A2440–A2463, 2016.

[15] W. E, J. Lu, and X. Yang. Asymptotic analysis of quantum dynamics in crystals: The Bloch-Wigner transform, Bloch dynamics and Berry phase. Acta Mathematicae Applicatae Sinica, English Series, Online First Articles, 2011.

[16] C. Fefferman and M. Weinstein. Honeycomb lattice potentials and Dirac points. *Journal of the American Mathematical Society*, 25(4):1169–1220, 2012.

[17] C. L. Fefferman and M. I. Weinstein. Wave packets in honeycomb structures and two-dimensional Dirac equations. *Comumunications in Mathematical Physics*, 326(1):251–286, 2014.

[18] P. Gérard, P. Markowich, N. Mauser, and F. Poupaud. Homogenization limits and Wigner transforms. *Communications on Pure and Applied Mathematics*, 50(4):323–379, 1997.

[19] J. Guillot, J. Ralston, and E. Trubowitz. Semi-classical asymptotics in solid state physics. *Communications in mathematical physics*, 116(3):401–415, 1988.

[20] G. A. Hagedorn. *Molecular Propagation through Electron Energy Level Crossings*. Number 536. American Mathematical Society, 1994.

[21] Z. Huang, S. Jin, P. Markowich, and C. Sparber. A Bloch decomposition-based split-step pseudospectral method for quantum dynamics with periodic potentials. *SIAM Journal on Scientific Computing*, 29(2):515–538, 2008.

[22] Z. Huang, S. Jin, P. A. Markowich, and C. Sparber. Numerical simulation of the nonlinear Schrödinger equation with multidimensional periodic potentials. *SIAM Multiscale Modeling and Simulation*, 7(2):539–564, 2008.

[23] S. Jin and P. Qi. A hybrid Schrödinger/Gaussian beam solver for quantum barriers and surface hopping. *Kinetic and Related Models*, 4(4):1097–1120, 2011.

[24] S. Jin, H. Wu, X. Yang, and Z. Huang. Bloch decomposition-based Gaussian beam method for the Schrödinger equation with periodic potentials. *Journal of Computational Physics*, 229(13):4869–4883, 2010.

[25] S. Jin, P. Markowich, and C. Sparber. Mathematical and computational methods for semiclassical Schrödinger equations. *Acta Numerica*, 20:121–209, 2011.

[26] C. F. Kammerer, C. Lasser, et al. Wigner measures and codimension two crossings. *Journal of Mathematical Physics*, 44(2):507–527, 2003.

[27] M. Katsnelson, K. Novoselov, and A. Geim. Chiral tunnelling and the klein paradox in graphene. *Nature physics*, 2(9):620–625, 2006.

[28] O. Klein. Die reflexion von elektronen an einem potentialsprung nach der relativistischen dynamik von dirac. *Zeitschrift für Physik*, 53(3-4):157–165, 1929.

[29] C. Lasser and S. Teufel. Propagation through conical crossings: an asymptotic semigroup. *Communications on Pure and Applied Mathematics*, 58(9):1188–1230, 2005.

[30] P. Markowich, N. Mauser, and F. Poupaud. A Wigner-function approach to (semi) classical limits: Electrons in a periodic potential. *Journal of Mathematical Physics*, 35(3):1066–1094, 1994.

[31] O. Morandi and L. Demeio. A wigner-function approach to interband transitions based on the multiband-envelope-function model. *Transport Theory and Statistical Physics*, 37(5-7):437–459, 2008.

[32] O. Morandi and M. Modugno. Multiband envelope function model for quantum transport in a tunneling diode. *Physical Review B*, 71(23):235331–235331, Jun 2005.

[33] A. C. Neto, F. Guinea, N. Peres, K. S. Novoselov, and A. K. Geim. The electronic properties of graphene. *Reviews of modern physics*, 81(1):109, 2009.

[34] G. Panati, H. Spohn, and S. Teufel. Effective dynamics for Bloch electrons: Peierls substitution and beyond. *Communications in Mathematical Physics*, 242(3):547–578, 2003.

[35] G. Panati, H. Spohn, and S. Teufel. Motion of electrons in adiabatically perturbed periodic structures. In A. Mielke, editor, *Analysis, Modeling and Simulation of Multiscale Problems*, pages 595–617. Springer-Verlag Berlin Heidelberg, 2006.

[36] T. Robinson. On Klein tunneling in graphene. *American Journal of Physics*, 80(2):141–147, 2012.

[37] N. Stander, B. Huard, and D. Goldhaber-Gordon. Evidence for Klein tunneling in graphene p-n junctions. *Physical Review Letters*, 102(2):026807, 2009.

[38] N. M. Tanushev, B. Engquist, and R. Tsai. Gaussian beam decomposition of high frequency wave fields. *Journal of Computational Physics*, 228(23):8856–8871, 2009.

[39] J. Tully and R. Preston. Trajectory surface hopping approach to nonadiabatic molecular collisions: the reaction of H with D. *The Journal of Chemical Physics*, 55(2):562–572, 1971.

[40] C. H. Wilcox. Theory of Bloch waves. *Journal d'Analyse Mathématique*, 33(1):146–167, 1978.

[41] A. F. Young and P. Kim. Quantum interference and Klein tunnelling in graphene heterojunctions. *Nature Physics*, 5(3):222–226, 2009.

[42] J. Zak. Dynamics of electrons in solids in external fields. *Physical Review*, 168(3):686, 1968.